intracellular activities may be useful in identifying CSCs.[9] For example, one property that may be useful in identifying stemness is 26S proteasome activity, which is involved in a diverse array of biological processes, including cell-cycle progression, DNA repair, apoptosis, and protein quality control.[10] Proteasome activity is significantly activated in cancer cells with proliferating and hypermetabolic activities, but generally suppressed in dormant states of stem cells.[11] Vlashi et al.[12] reported that human glioma and breast CSCs were identical to the subpopulation of cells monitored by green fluorescent protein ZsGreen fused to a degron motif of ornithine decarboxylase (ODC), which accumulated within the cell because of low 26S proteasome activity. Stem cells are also characterized by resistance to oxidative stress (superoxide) according to data obtained using the detoxifier system.[13] Hematopoietic stem cells contain a lower level of reactive oxygen species (ROS) than their mature progeny, and these differences are critical for maintaining stem cell function.[14] Human breast CSCs contain lower ROS levels, especially mitochondrial superoxide, than corresponding nontumorigenic cells.[15] In this study, we visualized two stem cell features, low proteasome activity and low ROS levels, in human HCC cells using the ZsGreen-fused degron sequence of ODC and the mitochondrial superoxide indicator MitoSOX Red, respectively. This monitoring system of stemness is a promising tool to elucidate the mechanism of progression and metastasis of human HCC.

Materials and Methods

Cell Culture. HCC cell lines (Hep3B, SK-Hep1, HuH7, and HLF) were purchased from the American Type Culture Collection (Manassas, VA) and the Human Science Research Resources Bank (Osaka, Japan). HuH7, Hep3B, and SK-Hep1 cells were cultured in log-growth phase in 1640 RPMI medium (Invitrogen, Carlsbad, CA), supplemented with 10% fetal bovine serum (Sigma-Aldrich, St. Louis, MO) and Pen/Strep (Sigma) as antibiotics. HLF cells were cultured in Dulbecco's modified Eagle's medium (DMEM; Invitrogen, Carlsbad, CA), supplemented with 10% fetal bovine serum and Pen/Strep, and grown in an incubator with 5% CO_2 at 37°C. Four HCC tumor samples were harvested at the time of surgery. After digestion with type IV collagenase (100 units/mL; Sigma) at 37°C for 15 minutes, the tissues were minced and the cell suspension was passed through a 100-μM nylon mesh and placed into DMEM medium. Cells were cultured in log-growth phase in DMEM medium (Invitrogen), supplemented with 10% fetal bovine serum (Sigma) and grown in an incubator with 5% CO_2 at 37°C.

Retroviral Transduction of the Degron Reporter Into Human HCC Cells. The degron sequence of ODC is known to be directly recognized by the proteasome, which leads to the immediate destruction of the involved protein. A retroviral expression vector pQCXIN-ZsGreen-cODC, containing green fluorescent ZsGreen-labeled degron ODC (Gdeg), was kindly provided by Dr. Frank Pajonk. The vector was transfected into platinum retroviral packaging cells and the retrovirus collected from the supernatant was used to infect HCC cells. Stable transfectants were selected with G418 (Invitrogen), and the accumulation of ZsGreen-degron ODC protein (Gdeg) was monitored by fluorescence microscopy and flow cytometry (FITC channel). Stable transfection was confirmed by exposing the cells to the proteasome inhibitor MG-132 (Calbiochem, San Diego, CA) for 12 hours. The established cell lines (HuH7, Hep3B, HLF, and SK-Hep1) as well as one cell culture line derived from each of the four HCC tissues were successfully engineered to stably express Gdeg. Fluorescence microscopy was performed using Axio-Observer (Carl Zeiss, Oberkochen, Germany), and images were acquired digitally using AxioVision (Carl Zeiss).

Flow Cytometry and Cell Sorting. For the flow cytometry experiments the cell number was evaluated using a FACSCanto II (BD Biosciences), and cell sorting was performed using a FACSAria II (BD Biosciences). HCC cells were washed with phosphate-buffered saline (PBS), then enzymatically dissociated using 0.05% trypsin-EDTA (Invitrogen). Trypsinized cells were suspended in fluorescence activated cell sorting (FACS) buffer and analyzed on a FACSCanto II using FACSDiva software (BD Biosciences). For intracellular ROS analysis, cells were loaded with 5 mM MitoSOX

Address reprint requests to: Shinji Tanaka, M.D., Ph.D., FACS, Department of Hepato-Biliary-Pancreatic Surgery, Graduate School of Medicine, Tokyo Medical and Dental University, 1-5-45 Yushima, Bunkyo-ku, Tokyo 113-8519, Japan. E-mail: shinji.msrg@tmd.ac.jp; fax: +81-3-5803-0263.

View this article online at wileyonlinelibrary.com.
DOI 10.1002/hep.26345
Potential conflict of interest: Nothing to report.
Additional Supporting Information may be found in the online version of this article.

Red (Invitrogen) at 37°C for 30 minutes and were immediately analyzed using FACSCanto II. $Gdeg^{high}ROS^{low}$ cells represented 0.16%-2.5% of the established HCC cell lines (Supporting Table 1). The percentage of $Gdeg^{high}ROS^{low}$ cells remained the same immediately after isolation by FACS, but increased to approximately 40% after time in culture (Supporting Fig. 4). For surface maker analysis, cells were labeled with allophycocyanin-conjugated antihuman CD44, CD90, EpCAM (BioLegend), and CD133/1 (MACS Miltenyi Biotec) antibodies. Labeled cells were immediately analyzed using FACSCanto II.

Time-Lapse Analysis. After FACS, $Gdeg^{high}$ or $Gdeg^{low}$ HCC cells were plated separately at a density of 10^4 cells in 6-cm dishes and in log-growth phase in 1640 RPMI medium (Invitrogen), supplemented with 10% fetal bovine serum (Sigma) and Pen/Strep (Sigma) as antibiotics. After incubation in 5% CO_2 at 37°C overnight, cell attachment was confirmed. Image analysis was performed using AxioVision and AxioObserver.

Treatment With Hypoxia or $CoCl_2$. HCC cells were exposed to hypoxic conditions (1% O_2, 5% CO_2, and 94% N_2) in an anaerobic workstation (Hirasawa Works, Tokyo, Japan). Oxygen concentration inside the workstation was constantly monitored by the oxygen sensor (MC-8G-S, Iijima Electrics, Gamagori, Japan) and maintained at 1% during the experiment. Cells (2.5×10^5) were grown with RPMI medium plus 3.5 g/L D-glucose in 10-cm dishes. The proportion of fluorescent cells was measured using FACSCanto II every 2 days. Cells were passaged every 6 days in an anaerobic workstation.

To further assess the effect of hypoxia on HCC cells, cells were treated with 100 μM $CoCl_2$ (Sigma) and/or 10 nM echinomycin (Sigma) added to the medium. After 24 and 48 hours, the proportion of fluorescence cells was measured using FACSCanto II. Chemosensitivity to the anticancer drug fluorouracil (5-FU) was analyzed using $Gdeg^{high}$ HuH7 and unsorted HuH7 cells under these hypoxia-mimicking condition. 5-FU was suspended in the culture media, serially diluted across 96-well microtiter plates (100 μL), and incubated at 37°C with 5% CO_2 for 48 hours. The number of living cells was measured using the MTS assay (Celltiter-Glo Luminescent Cell Viability Assay, Promega, Madison, WI), according to the manufacturer's instructions. The absorbance was read at 490 nm using a multiwell plate reader (Model 550, Bio-Rad, Richmond, CA), with wells containing medium but no cells serving as blank controls. Experiments were independently evaluated in triplicate.

Spheroid Assay. The spheroid assay was performed as described.[16] After FACS, $Gdeg^{high}$ or unsorted cells were plated separately at a density of 1,000 cells in low attachment plates (96-well Ultra Low Cluster Plate; Costar, Corning, NY) and incubated in serum-free DMEM/F12 medium (Invitrogen). For observation by time-lapse microscopy, 6-cm dishes were coated with poly-HEMA (20 mg/mL; Sigma). Image analysis was performed using AxioVision and AxioObserver.

Tumor Xenotransplantation and Tumorigenicity. Female NOD.CB17-PRkdc^{Scid}/J mice aged 4-6 weeks were purchased from Charles River Japan (Kanagawa, Japan). Various numbers of sorted $Gdeg^{high}ROS^{low}$ and unsorted HCC cells, ranging from 1×10^2 to 1×10^5 cells, were each mixed with 100 μL of Matrigel (BD Biosciences) and injected subcutaneously into both flanks of mice under anesthesia. Tumor formation was monitored every 2 days. All *in vivo* procedures were approved by the Animal Care Committee of Tokyo Medical and Dental University (Permission No. 090235).

RNA Extraction and Gene Expression Analysis. Total RNA was extracted from cancer and adjacent noncancerous tissues using the RNeasy kit (Qiagen, Hilden, Germany), and the integrity of obtained RNA was assessed using the Agilent 2100 Bioanalyzer (Agilent Technologies, Palo Alto, CA). All samples had an RNA Integrity Number greater than 5.0. Contaminant DNA was removed by digestion with RNase-free DNase (Qiagen). Complementary RNA was prepared from 2 μg of total RNA using 1-cycle target labeling and a control reagent kit (Affymetrix, Santa Clara, CA). Hybridization and signal detection of HG-U133 Plus 2.0 arrays (Affymetrix) were performed according to the manufacturer's instructions. The microarray datasets of (1) $Gdeg^{high}ROS^{low}$ and $Gdeg^{low}ROS^{high}$ HuH7 cells and (2) 253 tissue samples from HCC patients were normalized separately using the robust multiarray average method found in the R statistical software (v. 2.12.1) together with the Bioconductor package. Estimated gene-expression levels were obtained in log2-transformed values, and 62 control probe sets were removed for further analysis.

Gene Set Enrichment Analysis (GSEA). Biological functions associated with the malignant phenotype in HCC cells were investigated using GSEA v. 2.0.7 with MSigDB gene sets v. 3.0.[17] Probe sets marked as "present" by the Gene Expression Console software (Affymetrix) in at least one $Gdeg^{high}ROS^{low}$ or $Gdeg^{low}ROS^{high}$HuH7 cell were used for this analysis. Gene set category "C2 CP REACTOME," which is

based on the Reactome database (http://www.reactome.org), was used. For analysis of the gene expression profiles obtained from HCC patients, a custom gene set was employed using genes showing more than a 2-fold change between $Gdeg^{high}ROS^{low}$ and $Gdeg^{low}ROS^{high}$ HuH7 cells. Gene sets satisfying both criteria with $P < 0.05$ and a false discovery rate (FDR) <0.05 were considered significant.

Macrophage Migration Assay. To determine whether tumor cells induce macrophage/monocyte chemotaxis, the double chamber migration assay was performed using the RAW264 murine macrophage cell line (RIKEN Cell Resource Center, Tsukuba, Japan). Briefly, the migration of RAW264 cells was assayed using a transwell chamber (24-well plate, 8-μm pore; BD Biosciences, Bedford, MA). In the lower chamber, 7.5×10^4 tumor cells in 0.8 mL of media were seeded and incubated in serum-free media for 72 hours. RAW264 cells (5×10^4 in 0.3 mL serum free media) were then seeded into the upper chamber and incubated at 37°C for 4 hours. RAW264 cells found on the upper surface of the filter were removed using a cotton wool swab. Cells were then fixed with 100% methanol and stained using Giemsa solution and the number of cells migrating to the lower surface was counted. Each experiment was conducted in triplicate and the mean is shown.

Peritoneal Metastasis Model. Peritoneal metastatic potentials of cancer cells were assessed as reported.[18] Briefly, 10^5 $Gdeg^{high}ROS^{low}$ HCC cells or unsorted control cells were injected intraperitoneally into 5-week-old female NOD.CB17-$PRkdc^{Scid}$/J mice (n = 4 mice per group; Charles River Japan, Kanagawa, Japan). The care and use of animals was in accordance with institutional guidelines. The mice were monitored three times weekly for lethargy, weight loss, and abdominal enlargement. Mice were euthanized by cervical dislocation at 4 weeks and the number and weight of tumor nodules within the peritoneal cavity were counted.

Immunofluorescent Staining. Tissue sections were prepared according to standard procedures. After deparaffinization, slides were incubated in permeabilization buffer (0.2% Triton-PBS) for 30 minutes, followed by incubation in blocking buffer (3% bovine serum albumin [BSA]-PBS) for 1 hour and exposure to the primary antibodies (F4/80 1:200, BioLegend) overnight at 4°C. Sections were then treated for 30 minutes with the secondary antibody Alexa Fluor 568 tetramethylrhodamine isothiocyanate-conjugated anti-rat IgG (1:1,000, Sigma) and Hoechst 33342 solution for nuclear staining diluted in PBS and 3% BSA. After mounting the slides were visualized with a fluorescent microscope (Carl Zeiss, Germany).

Protein Network Analysis. To reveal functional relationships among genes differentially expressed in $Gdeg^{high}ROS^{low}$ HuH7 cells, the protein interaction network was analyzed. Genes up-regulated or down-regulated more than 1.1-fold between $Gdeg^{high}ROS^{low}$ and $Gdeg^{low}ROS^{high}$HuH7 cells were included in the network. Protein interaction data obtained from BIND (http://bond.unleashedinformatics.com), BioGRID (http://thebiogrid.org), and HPRD (http://www.hprd.org) were downloaded from the ftp site of the National Center for Biotechnology Information (NCBI; ftp://ftp.ncbi.nih.gov/gene/GeneRIF/interactions.gz). The protein interaction network was analyzed using Cytoscape software.[19]

Patients and Tissue Samples. In all, 187 patients underwent curative hepatectomy for HCC from 2004 to 2007 at Tokyo Medical and Dental University Hospital (Tokyo, Japan), and among these, 153 cases were randomly selected for this study. With Institutional Review Board approval, written informed consent was obtained from all patients (Permission No. 1080). Noncancerous liver tissue adjacent to HCC (n = 100) was snap-frozen in liquid nitrogen and stored at −80°C. Patients were followed up with assays for serum alpha-fetoprotein levels and protein induced by vitamin K absence or antagonists-II every month and with ultrasonography, computed tomography, and magnetic resonance imaging every 3 months. Median observation time was 9.86 months.

To divide patients into subgroups based on expression profiles of a particular gene set, gene-set enrichment patterns were analyzed using a method similar to that described by Ben-Porath et al.[20] For each patient, the number of genes that showed more than a 1.1-fold change in expression (either up-regulation or down-regulation) compared to the mean expression levels were counted. Patients who exhibited up-regulation of more than 30% of the genes in the gene set were classified as the high expression group. Likewise, patients who showed down-regulation of more than 30% of the genes in the gene set were classified as the low expression group. Samples that satisfied neither or both criteria above were classified as the moderate expression group. The recurrence-free survival rates among three groups were compared by Kaplan-Meier curves, followed by the log-rank test.

Statistical Analysis. Experimental data are expressed as mean values with 95% confidence intervals (CI) and were compared using a two-sided paired Student's t test. Statistical significance was defined as $P < 0.05$.

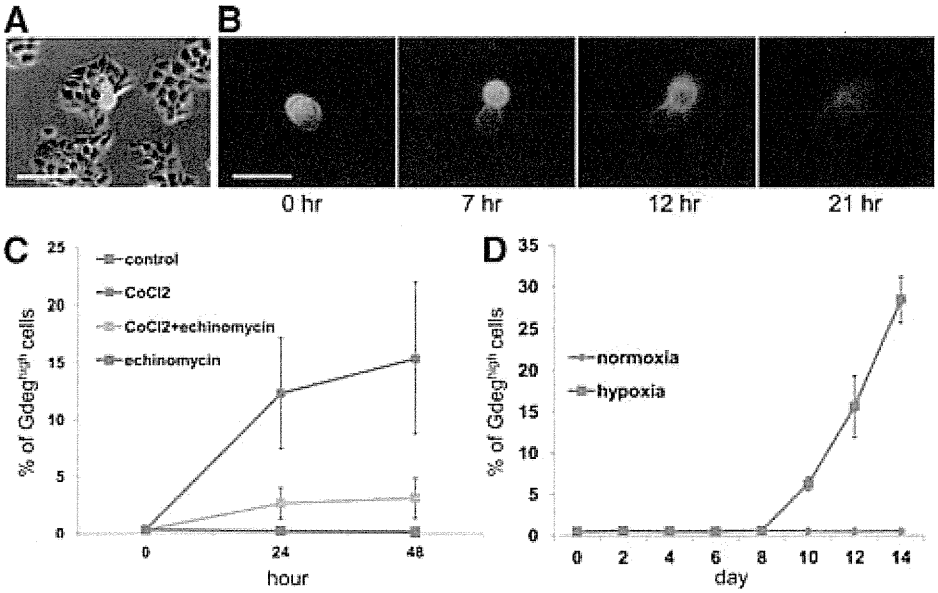

Fig. 1. (A) Frequency of cells with accumulation of Gdeg protein ($Gdeg^{high}$) in human HCC cultures (bar, 100 μm). (B) Asymmetric cell division of the $Gdeg^{high}$ HCC observed by time-lapse microscope. $Gdeg^{high}$ HCC cells asymmetrically divided into $Gdeg^{high}$ and $Gdeg^{low}$ HCC cells (bar, 50 μm). (C) The alteration of the $Gdeg^{high}$ proportion in the unsorted HCC cells after 24-hour and 48-hour treatment of $CoCl_2$ (100 μM) with or without echinomycin (10 nM); results are presented as means ± standard deviation from triplicate experiments. (D) The alteration of the $Gdeg^{high}$ proportion in the unsorted HCC cells under long-term hypoxic conditions (1% O_2); results are presented as means ± standard deviation from triplicate experiments.

Results

Characterization of CSC Proteasome Activity in Human HCC Cells. Human HCC cells were engineered to stably express ZsGreen-labeled degron (Gdeg) according to the previous report by Vlashi et al.[12] Cells displaying high levels of Gdeg ($Gdeg^{high}$) represented 0.5%-7.5% of the population in human HCC cell lines (Fig. 1A). In contrast, $Gdeg^{high}$ cells represented 0.1% of the population in human primary HCC (Supporting Fig. 1); however, only four generations were passaged without establishment. Isolation of the established $Gdeg^{high}$ cells and $Gdeg^{low}$ cells was performed using FACSAria II (BD Biosciences). As demonstrated by time-lapse microscopy, $Gdeg^{high}$ cells can asymmetrically divide into $Gdeg^{low}$ and $Gdeg^{high}$ cells, while $Gdeg^{low}$ cells never divide into $Gdeg^{high}$ cells. These results demonstrate some properties of CSCs and non-CSCs,[21] such as hierarchical division of CSCs and loss of stemness in differentiated non-CSCs (Fig. 1B; Supporting Video 1). In addition, the spheroid assay revealed that $Gdeg^{high}$ cells form slightly larger spheroids than unsorted cells (Supporting Fig. 2).

Effects of Hypoxia on HCC CSCs. Since pluripotent potentials in embryonic stem cells can be efficiently maintained under low oxygen levels[22] and hypoxia can contribute to CSC maintenance,[23] the effects of hypoxic conditions in unsorted HCC cells transfected with Gdeg were analyzed. The proportion of $Gdeg^{high}$ HCC cells significantly increased after 48-hour treatment with $CoCl_2$, an agent mimicking the activation of hypoxia-inducing factor (HIF).[24] The effects of $CoCl_2$ were blocked by echinomycin, a molecule inhibiting HIF-1 DNA binding activity (Fig. 1C) that has recently been reported to eradicate serially transplantable human acute myeloid leukemia (AML) in xenogeneic models by preferential elimination of CSCs.[25] The effects of long-term hypoxic treatment (1% O_2) were also analyzed in the unsorted HCC cells. $Gdeg^{high}$ cells represented 0.5% of the population on Day 1, but significantly increased to 28.0% on Day 14 (Fig. 1D). Similar to previous reports showing that CSCs are usually resistant to the conventional chemotherapy,[9] $Gdeg^{high}$ cells also demonstrated chemoresistance compared to unsorted cells under hypoxia conditions (Supporting Fig. 3). These results are consistent with reports showing that hypoxic conditions serve as a stimulus to reprogram cells towards normal stem cells and CSCs.[22,23]

CSCs Property of the HCC Subpopulation With Low Intracellular ROS Levels and Low Proteasome Activity. $Gdeg^{high}$ cells had a lower concentration of ROS than the unsorted cells based on the intracellular concentrations of MitoSOX Red staining. Intracellular ROS-positive cells (ROS^{high}) accounted for 71.0% ± 8.22% of the unsorted HuH7 HCC cells, but only

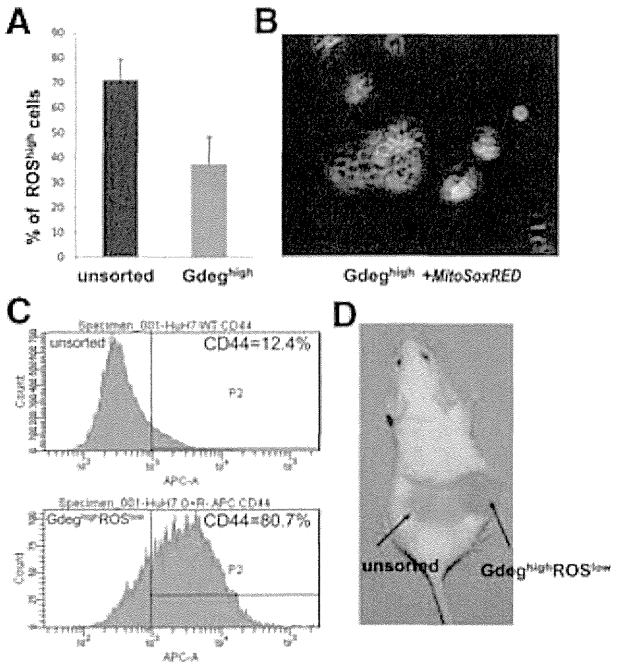

Fig. 2. (A) The proportion of ROS-positive cells (ROS^{high}) in unsorted HCC cells (left) and the sorted $Gdeg^{high}$ HCC cells (right) determined by FACS analysis with MitoSOX Red staining; results are presented as means ± standard deviation from triplicate experiments ($P < 0.05$). (B) $Gdeg^{high}$ and $Gdeg^{high}$ HCC cells stained with MitoSOX Red; (C) Flow cytometry histogram showing expression of CD44 positive cells in the $Gdeg^{high}ROS^{low}$ HuH7 cells (80.7%) and unsorted HuH7 cells (12.4%). (D) Tumorigenicity analysis using NOD/SCID mice; a tumor nodule was detected at the inoculation site of 10^2 $Gdeg^{high}ROS^{low}$ HCC cells, but not at the inoculation site of the unsorted cells.

37.2% ± 10.8% within the $Gdeg^{high}$ HuH7 cell population ($P < 0.05$). The $Gdeg^{high}$ group also contained a subpopulation of cells with low intracellular ROS levels ($Gdeg^{high}ROS^{low}$) (Fig. 2A).

To determine whether $Gdeg^{high}ROS^{low}$ HCC cells might possess certain stem cell-like properties, the expression of stem cell surface markers, CD133,[5] CD90,[6] EpCAM,[7] and CD44 was analyzed.[8] CD44-postiveness was detected in 80.7% of $Gdeg^{high}ROS^{low}$ HuH7 cells, but in only 12.4% of unsorted HuH7 cells (Fig. 2C). EpCAM and CD90 expression were increased in the $Gdeg^{high}ROS^{low}$ HLF cells compared to the unsorted HLF cells (EpCAM; 6.0% versus 2.7%, CD90; 55.9% versus 44.6%).

An important test for validating whether cells are CSCs is the identification of a cancer initiation population demonstrated by increased tumorigenicity *in vivo*. Different cell numbers from each population were injected subcutaneously into nonobese diabetic / severe combined immunodeficient (NOD/SCID) mice in numbers ranging from 10^2 to 10^5 cells per injection. $Gdeg^{high}ROS^{low}$ HCC cells had higher tumorigenic capacity than unsorted cells. As few as 10^2 $Gdeg^{high}ROS^{low}$ HCC cells could form a subcutaneous tumor (Fig. 2D, Table 1; Supporting Table 2). Cancer initiation frequency was calculated using L-Calc Software[26] (Stem Cell Technologies), and significance was determined by chi-square analysis using ELDA (Walter and Eliza Hall Bioinformatics).[26] The cancer initiation frequency was 1 in 2,083 (95% CI = 739 to 5,867) for $Gdeg^{high}ROS^{low}$ HCC cells and 1 in 79,189 (95% CI = 31,651 to 198,128) for unsorted cells ($P < 0.001$). These data validate that CSCs are significantly enriched in the $Gdeg^{high}ROS^{low}$ subpopulation compared to unsorted HCC cells.

Tumor-Host Interactions of HCC CSCs. Comprehensive gene expression analysis in $Gdeg^{high}ROS^{low}$ HCC cells was performed to acquire the CSC gene profile. As described in a previous report,[13] GSEA based on the Reactome database[27] was utilized to determine the biological pathways activated or inactivated in $Gdeg^{high}ROS^{low}$ HCC cells. The GSEA demonstrated significant enrichment in 8 gene sets (Supporting Table 3), and the gene set "chemokine_receptors_bind_chemokines" showed the lowest FDR (Fig. 3A). A protein interaction network was then constructed using 12,890 probe sets with at least 10% change in expression levels. To more closely investigate molecular networks associated with chemokines, a subnetwork of 2-hop neighbors from chemokine ligands and receptors including CXCL, CCL, CX3CL, XCL, CXCR, CCR, CX3CR, and XCR family genes was generated (Fig. 3B).

The ability of $Gdeg^{high}ROS^{low}$ HCC cells to induce macrophage chemotaxis was determined using a chemotaxis assay and the RAW264 murine macrophage-like cell line (Fig. 3C). $Gdeg^{high}ROS^{low}$ HCC cells significantly facilitated RAW264 cell migration compared to their counterparts and unsorted controls (average number of cells that migrated to the lower chamber, $Gdeg^{high}ROS^{low}$ HCC cells versus unsorted HCC cells: difference = 192, 95% CI = 61 to 323, $P = 0.0153$, n = 3; $Gdeg^{high}ROS^{low}$ HCC cells versus $Gdeg^{low}ROS^{high}$ HCC cells: difference = 196, 95%

Table 1. Enhanced Tumor Formation by $Gdeg^{high}ROS^{low}$ HCC Cells

	Fraction (%) of Injected Mice That Developed Tumors	
Number of Cells Injected	Injected With $Gdeg^{high}ROS^{low}$ Cells	Injected With Unsorted Cells
10^2	3/6 (50%)	0/6 (0%)
10^3	4/6 (66.7%)	1/6 (16.7%)
10^4	5/6 (83.3%)	2/6 (33.3%)
10^5	5/6 (83.3%)	3/6 (50%)

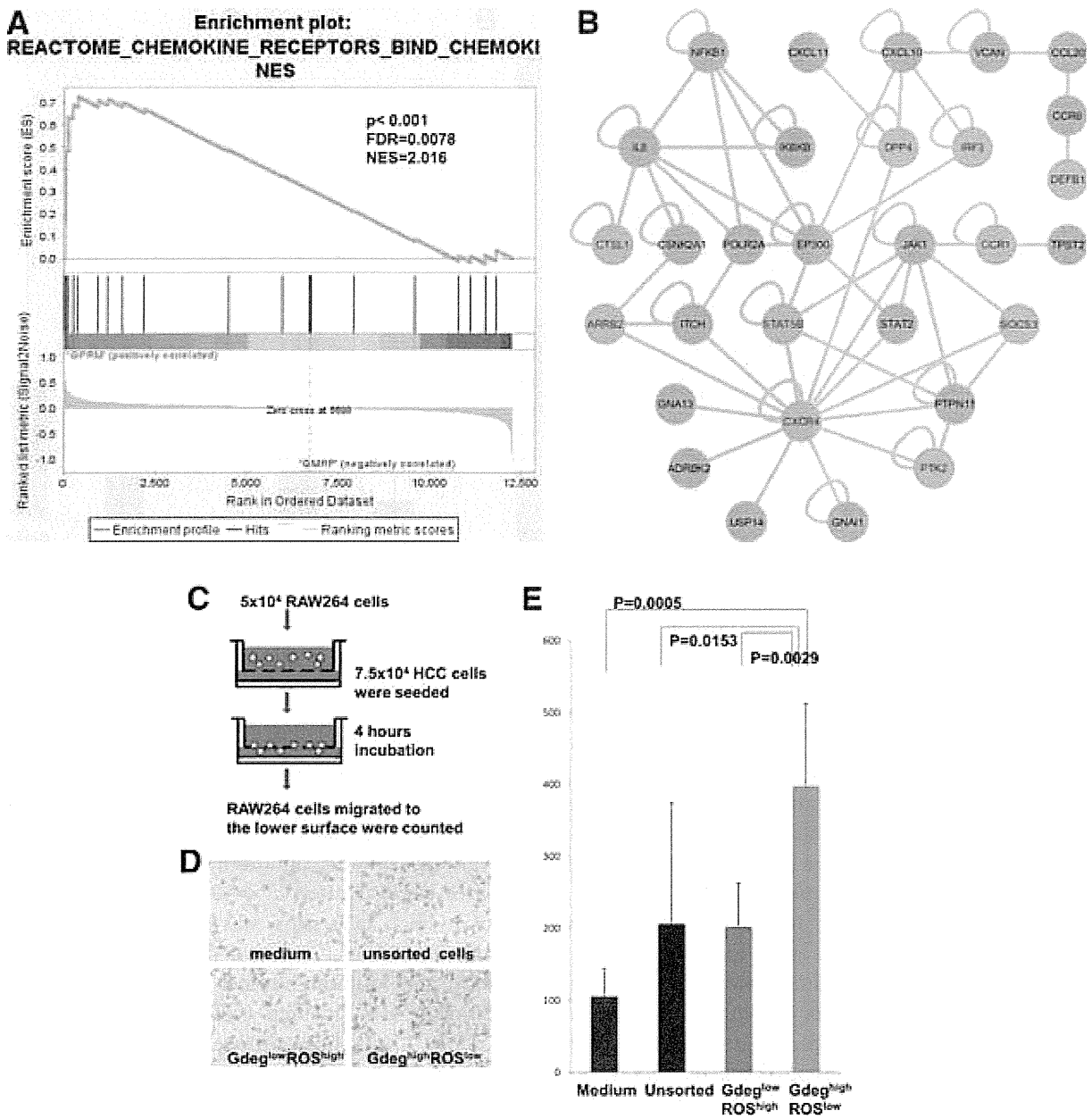

Fig. 3. (A) GSEA evaluation of gene-expression profile associated with Gdeg^{high}ROS^{low} HCC cells; the gene set "chemokine_receptors_bind_-chemokines" showed the lowest FDR ($P < 0.001$; FDR = 0.0078; NES = 2.016). (B) A protein interaction network constructed using 12,890 probe sets with at least 10% change in expression levels; a sub-network of 2-hop neighbors from chemokine ligands and receptors was extracted. (C) Diagram of the double chamber migration assay using a RAW264 murine macrophage-like cell line. (D) Giemsa staining for the RAW264 cells migrating to the lower surface. (E)The number of the RAW264 cells migrated to the lower surface induced by Gdeg^{high}ROS^{low} HCC cells compared to Gdeg^{low}ROS^{high} HCC cells, unsorted HCC cells, and medium. Each experiment was conducted in triplicate, and data are presented as the means ± 95% CI.

CI = 112 to 280, $P = 0.0029$, n = 3, Gdeg^{high}ROS^{low} HCC cells versus medium: difference = 292, 95% CI = 214 to 370, $P < 0.001$, n = 3) (Fig. 3D,E). Facilitated migration of host macrophages may be associated with niche formation of the HCC CSCs subpopulation.

To investigate whether the HCC cells established *in vivo* metastasis, Gdeg^{high}ROS^{low} or unsorted HCC cells were administered intraperitoneally in a NOD/SCID mouse model, as described previously.[18] Peritoneal metastases were assessed by counting the number of nodules and evaluating tumor weight in the mesentery and peritoneal walls. The tumor weight (average weight of dissemination nodules: Gdeg^{high}ROS^{low} HCC cells versus unsorted HCC cells, difference = 0.197, 95% CI = −0.304 to 0.699, $P = 0.3728$,

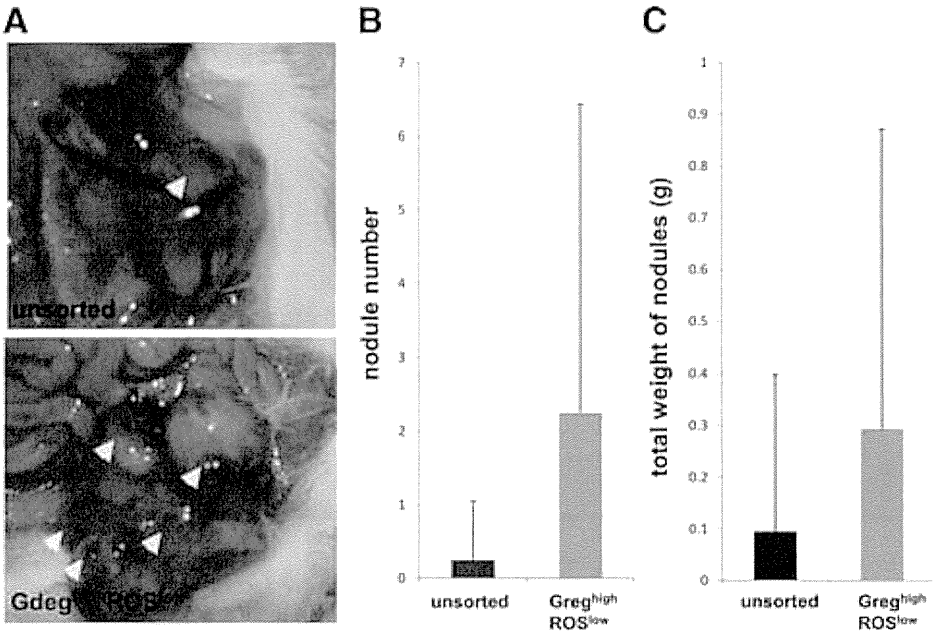

Fig. 4. (A) Macroscopic appearance of peritoneal metastases on day 28 after intraperitoneal injection of 10^5 HCC cells (Upper, unsorted HuH7 cells; Lower, $Gdeg^{high}ROS^{low}$ HuH7 cells). The capacity of $Gdeg^{high}ROS^{low}$ HCC cells to establish peritoneal metastases was assessed by (B) counting the number of nodules, and (C) evaluating tumor weight in the mesentery and peritoneal walls compared to the unsorted cells. Four mice were used in each group. Each value represents the mean ± 95% CI.

n = 4; Fig. 4B) and number (average number of dissemination nodules: $Gdeg^{high}ROS^{low}$ HCC cells versus unsorted HCC cells, difference = 2.00, 95% CI = −1.28 to 5.28, $P = 0.1857$, n = 4; Fig. 4C) of the $Gdeg^{high}ROS^{low}$ HCC cells group were higher than those in the unsorted group. Immunofluorescent analysis revealed that murine macrophages had infiltrated around the $Gdeg^{high}$ HCC cells located at the metastatic tumor margins, indicative of the ability of these cells to recruit macrophages *in vivo* (Fig. 5).

Clinical Implication of the Gene Signature Up-Regulated in HCC CSCs. The clinical implication of the HCC CSC gene signature was retrospectively assessed using liver tissues from patients who received curative resection of HCC. CSC-gene signatures were generated as 43 probe sets using the gene expression profiles up-regulated in $Gdeg^{high}ROS^{low}$ HCC cells (Supporting Table 4) and revealed a significant correlation between the noncancerous liver gene expressions and the CSC-gene signatures ($P = 0.004$ and FDR = 0.005; Fig. 6A). CSC-gene signatures were then evaluated with regard to patient outcomes. Patients were divided into three subtypes; high, moderate, and low expression groups, on the basis of expression profiles of the 43 CSC-related probe sets (Fig. 6B). These three groups showed significant differences in recurrence-free survival rates ($P = 0.002$ by log-rank test; Fig. 6C). High expression was significantly associated with diminished liver function (low albumin and high bilirubin) and tumor number (Supporting Fig. 5). Expression of CSC markers (CD133, EpCAM, CD44, and CD90)[5-8] and biliary/progenitor cell markers (cytokeratin 7 and cytokeratin 19)[28] was also up-regulated in the high expression group (Supporting Fig. 6).

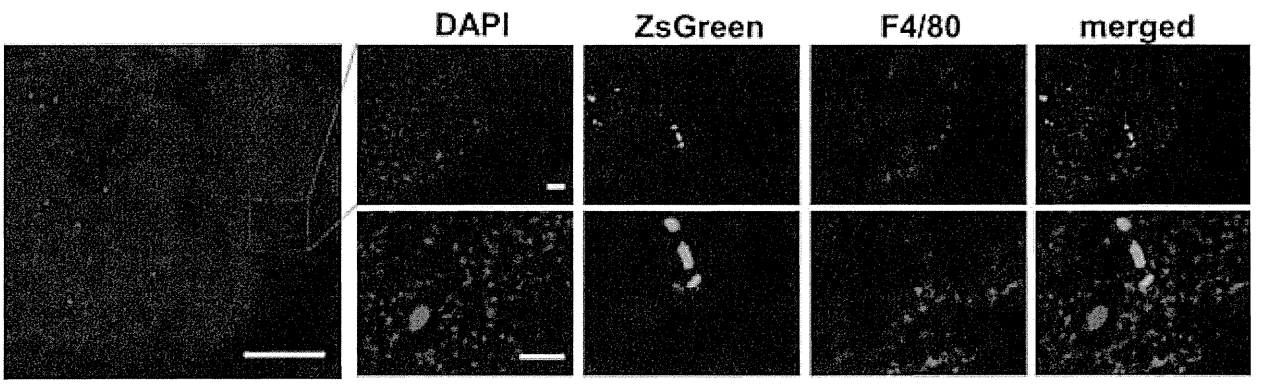

Fig. 5. Immunofluorescence of metastatic tumor sections labeled with antimouse F4/80 (bars, 1,000 μm (white) and 100 μm (yellow)); murine macrophages infiltrated around the $Gdeg^{high}$ HuH7 cells located at the margins of the metastatic tumors.

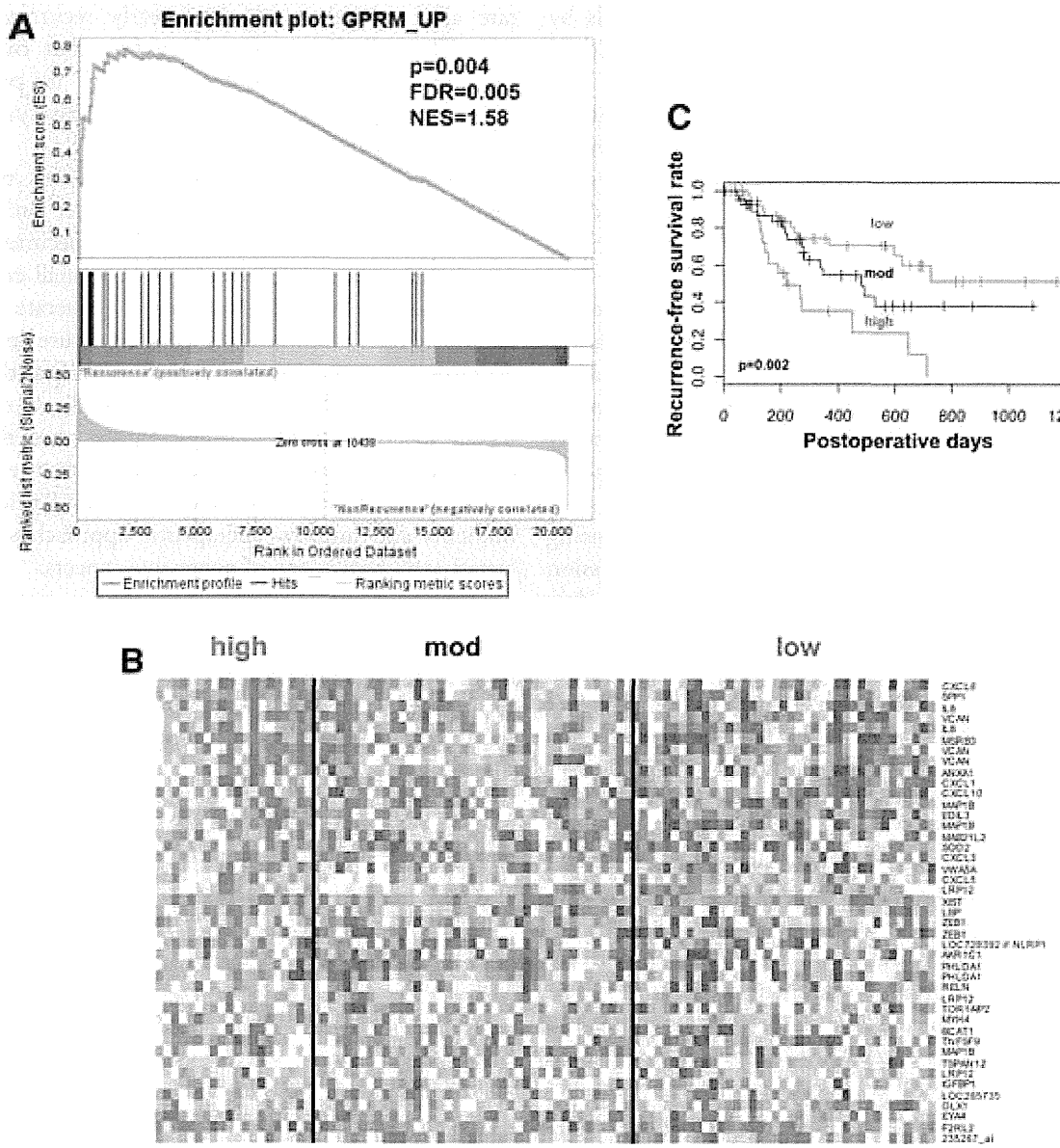

Fig. 6. (A) GSEA evaluation of the adjacent nontumor tissues; a positive correlation was observed between the gene set of Gdeg^{high}ROS^{low} HCC gene signature and noncancerous liver gene expression ($P < 0.004$; FDR = 0.005; NES = 1.58). (B) Patients were divided into three subtypes based on the expression profiles of 43 up-regulated probe sets of Gdeg^{high}ROS^{low} HCC. (C) A significant correlation was observed between the Gdeg^{high}ROS^{low} HCC gene signature and the recurrence-free survival rates of the patients after curative resection of HCC ($P = 0.002$).

Recently, leukemia CSC-specific gene signatures were revealed as highly independent predictors of patient survival.[29] This gene signature analysis demonstrates the clinical significance of identifying CSC populations in HCC using the stem-cell monitoring system described here.

Discussion

The monitoring system of stemness proposed here visualized two stem cell features, low proteasome activity and low ROS levels, in human HCC. Monitoring HCC proteasome activity revealed that human HCC cells contain a small population of cells that undergo asymmetric division, exhibiting the multipotency and self-renewal of CSCs (Fig. 1B).[20] Next, we showed that $CoCl_2$, an agent mimicking the activation of HIF,[24] increased the proportion of Gdeg^{high} HCC cells, indicative of low proteasome activity, while echinomycin, a molecule that inhibits HIF-1 DNA binding activity, blocked this effect (Fig. 1C). Recently, echinomycin was also reported to eradicate serially

transplantable human AML in xenogeneic models by preferential elimination of CSCs.[25] Similar to $CoCl_2$ treatment, hypoxic conditions also increased the proportion of $Gdeg^{high}$ HCC cells (Fig. 1D), consistent with a previous report indicating that hypoxia serves as a stimulus to reprogram cells towards normal stem cells[22] and CSCs.[23] Additionally, HCC cells had an ROS concentration lower than that of unsorted HCC cells, including a subpopulation of $Gdeg^{high}$ HCC cells ($Gdeg^{high}ROS^{low}$), in agreement with a previous report showing that normal stem cells and CSCs contain a lower concentration of ROS than their more mature progeny.[14] Importantly, xenotransplantation experiments revealed that cells with increased tumorigenicity were significantly concentrated in the subpopulation of $Gdeg^{high}ROS^{low}$ HCC cells.

An HCC stem cell-specific signature (Supporting Table 4) was identified by genome-wide expression analysis, and GSEA based on the Reactome data base[27] showed that our HCC stem cell system significantly correlated with the chemokine network (Fig. 3A,B; Supporting Table 3). Inflammatory mediators and cells are indispensable components of tumor-host interactions,[30] and studies have shown that cancer cell-secreted factors generate an inflammatory niche hospitable for progression and metastasis of cancer.[31,32] More recent studies have shown that glioma-initiating cells produced inflammatory mediators such as chemokines that induce tumor-associated macrophages to organize the glioma-initiating cells niche.[33] Macrophages are an important component of the tumor-host interaction that controls the survival, migration, and growth of metastatic cells.[34] Our data showed that $Gdeg^{high}ROS^{low}$ HCC cells induced macrophage chemotaxis more effectively than their counterparts (Fig. 3E). Furthermore, these cells had a higher capacity for dissemination in an *in vivo* peritoneal metastasis model (Fig. 4B,C). We also found macrophage infiltration around the CSCs located at the margin of the dissemination tumor (Fig. 5), indicative of the ability of HCC CSCs to recruit macrophages *in vivo*.

Recent studies on murine breast CSCs have revealed that the tumor-host interaction plays a critical role in metastatic colonization of cancer cells.[35] It is noteworthy that the tumor-host interaction mediated by HCC CSCs is potentially associated with metastatic initiation in our study. The host gene expression signature of the noncancerous microenvironment is closely associated with prediction of HCC recurrence[36] and lung adenocarcinoma.[37] As a result, the gene expression signature of our HCC stem cells (Supporting Table 4) significantly correlates with the disease-free survival rate after radical surgery and early recurrence (Fig. 6A). These findings strongly suggest that our HCC stem cell monitoring system is useful in predicting clinical prognosis, and the validity of this system was further confirmed (Fig. 6C).

Our HCC CSCs system, which monitors two stem cell features, is a promising tool to extract and identify CSCs in live bodies and histological specimens. This system demonstrated the presence of a small cell population with an increased capacity to generate dissemination *in vivo*. Clinically, the gene signature specifically expressed in our HCC stem cells significantly correlated with HCC recurrence after radical resection. Taken together, these findings suggest that this stem cell monitoring system could illuminate the *in vivo* significance of CSC-host interactions and microenvironments and improve therapeutic approaches for metastasis and recurrence of aggressive cancers.

Acknowledgment: The authors thank Drs. Frank Pajonk and Erina Vlashi at the University of California for providing the pQCXIN-ZsGreen-cODC plasmid, Dr. Hideshi Ishii at Osaka University for providing the primary HCC cell cultures, and Ms. Ayumi Shioya for technical assistance.

References

1. Zhu AX, Duda DG, Sahani DV, Jain RK. HCC and angiogenesis: possible targets and future directions. Nat Rev Clin Oncol 2011;8: 292-301.
2. Arii S, Yamaoka Y, Futagawa S, Inoue K, Kobayashi K, Kojiro M, et al. Results of surgical and nonsurgical treatment for small-sized hepatocellular carcinomas: a retrospective and nationwide survey in Japan. The Liver Cancer Study Group of Japan. HEPATOLOGY 2000;32: 1224-1229.
3. Shrager B, Jibara G, Schwartz M, Roayaie S. Resection of hepatocellular carcinoma without cirrhosis. Ann Surg 2012;255:1135-1143.
4. Reya T, Morrison SJ, Clarke MF, Weissman IL. Stem cells, cancer, and cancer stem cells. Nature 2001;414:105-111.
5. Ma S, Chan KW, Hu L, Lee TK, Wo JY, Ng IO, et al. Identification and characterization of tumorigenic liver cancer stem/progenitor cells. Gastroenterology 2007;132:2542-2556.
6. Yang ZF, Ho DW, Ng MN, Lau CK, Yu WC, Ngai P, et al. Significance of CD90+ cancer stem cells in human liver cancer. Cancer Cell 2008;13:153-166.
7. Yamashita T, Ji J, Budhu A, Forgues M, Yang W, Wang HY, et al. EpCAM-positive hepatocellular carcinoma cells are tumor-initiating cells with stem/progenitor cell features. Gastroenterology 2009;136: 1012-1024.
8. Zhu Z, Hao X, Yan M, Yao M, Ge C, Gu J, et al. Cancer stem/progenitor cells are highly enriched in CD133+CD44+ population in hepatocellular carcinoma. Int J Cancer 2010;126:2067-2078.
9. Clevers, H. The cancer stem cell: premises, promises and challenges. Nat Med 2011;17:313-319.
10. Murata S, Yashiroda H, Tanaka K. Molecular mechanisms of proteasome assembly. Nat Rev Mol Cell Biol 2009;10:104-115.
11. Hernebring M, Brolén G, Aguilaniu H, Semb H, Nyström T. Elimination of damaged proteins during differentiation of embryonic stem cells. Proc Natl Acad Sci U S A 2006;103:7700-7705.

12. Vlashi E, Kim K, Lagadec C, Donna LD, McDonald JT, Eghbali M, et al. In vivo imaging, tracking, and targeting of cancer stem cells. J Natl Cancer Inst 2009;101:350-359.
13. Tanaka S, Mogushi K, Yasen M, Ban D, Noguchi N, Irie T, et al. Oxidative stress pathways in noncancerous human liver tissue to predict hepatocellular carcinoma recurrence: a prospective, multicenter study. HEPATOLOGY 2011;54:1273-1281.
14. Merchant AA, Singh A, Matsui W, Biswal S. The redox-sensitive transcription factor Nrf2 regulates murine hematopoietic stem cell survival independently of ROS levels. Blood 2011;118:6572-6579.
15. Diehn M, Cho RW, Lobo NA, Kalisky T, Dorie MJ, Kulp AN, et al. Association of reactive oxygen species levels and radioresistance in cancer stem cells. Nature 2009;458:780-783.
16. Adikrisna R, Tanaka S, Muramatsu S, Aihara A, Ban D, Ochiai T, et al. Identification of pancreatic cancer stem cells and selective toxicity of chemotherapeutic agents. Gastroenterology 2012;143:234-45.
17. Subramanian A, Tamayo P, Mootha VK, Mukherjee S, Ebert BL, Gillette MA, et al. Gene set enrichment analysis: a knowledge-based approach for interpreting genome-wide expression profiles. Proc Natl Acad Sci U S A 2005;102:15545-15550
18. Tanaka S, Pero SC, Taguchi K, Shimada M, Mori M, Krag DN, et al. Specific peptide ligand for Grb7 signal transduction protein and pancreatic cancer metastasis. J Natl Cancer Inst 2006;98:491-498.
19. Smoot ME, Ono K, Ruscheinski J, Wang PL, Ideker T. Cytoscape 2.8: new features for data integration and network visualization. Bioinformatics 2011;27:431-432.
20. Ben-Porath I, Thomson MW, Carey VJ, Ge R, Bell GW, Regev A, et al. An embryonic stem cell-like gene expression signature in poorly differentiated aggressive human tumors. Nat Genet 2008;40:499-507.
21. Knoblich JA. Asymmetric cell division: recent developments and their implications for tumour biology. Nat Rev Mol Cell Biol 2010;11: 849-860.
22. Yoshida Y, Takahashi K, Okita K, Ichisaka T, Yamanaka S. Hypoxia enhances the generation of induced pluripotent stem cells. Cell Stem Cell 2009;5:237-241.
23. Li Z, Bao S, Wu Q, Wang H, Eyler C, Sathornsumetee S, et al. Hypoxia-inducible factors regulate tumorigenic capacity of glioma stem cells. Cancer Cell 2009;15:501-513.
24. Pacary E, Legros H, Valable S, Duchatelle P, Lecocq M, Petit E, et al. Synergistic effects of $CoCl_2$ and ROCK inhibition on mesenchymal stem cell differentiation into neuron-like cells. J Cell Sci 2006;119: 2667-2678.
25. Wang Y, Liu Y, Malek SN, Zheng P, Liu Y. Targeting HIF1α eliminates cancer stem cells in hematological malignancies. Cell Stem Cell 2011;8: 399-411.
26. Ishizawa K, Rasheed ZA, Karisch R, Wang Q, Kowalski J, Susky E, et al. Tumor-initiating cells are rare in many human tumors. Cell Stem Cell 2010;7:279-282.
27. Croft D, O'Kelly G, Wu G, Haw R, Gillespie M, Matthews L, et al. Reactome: a database of reactions, pathways and biological processes. Nucleic Acids Res 2011;39:D691-697.
28. Durnez A, Verslype C, Nevens F, Fevery J, Aerts R, Pirenne J, et al. The clinicopathological and prognostic relevance of cytokeratin 7 and 19 expression in hepatocellular carcinoma. A possible progenitor cell origin. Histopathology 2006;49:138-151.
29. Eppert K, Takenaka K, Lechman ER, Waldron L, Nilsson B, van Galen P, et al. Stem cell gene expression programs influence clinical outcome in human leukemia. Nat Med 2011;17:1086-1093.
30. Mantovani A, Allavena P, Sica A, Balkwill F. Cancer-related inflammation. Nature 2008;454:436-444.
31. Kim S, Takahashi H, Lin WW, Descargues P, Grivennikov S, Kim Y, et al. Carcinoma-produced factors activate myeloid cells through TLR2 to stimulate metastasis. Nature 2009;457:102-106.
32. Karnoub AE, Dash AB, Vo AP, Sullivan A, Brooks MW, Bell GW, et al. Mesenchymal stem cells within tumour stroma promote breast cancer metastasis. Nature 2007;449:557-563.
33. Yi L, Xiao H, Xu M, Ye X, Hu J, Li F, et al. Glioma-initiating cells: a predominant role in microglia/macrophages tropism to glioma. J Neuroimmunol 2011;232:75-82.
34. Qian B, Deng Y, Im JH, Muschel RJ, Zou Y, Li J, et al. A distinct macrophage population mediates metastatic breast cancer cell extravasation, establishment and growth. PLoS One 2009;4:e6562.
35. Malanchi I, Santamaria-Martínez A, Susanto E, Peng H, Lehr HA, Delaloye JF, et al. Interactions between cancer stem cells and their niche govern metastatic colonization. Nature 2011;481:85-89.
36. Budhu A, Forgues M, Ye QH, Jia HL, He P, Zanetti KA, et al. Prediction of venous metastases, recurrence, and prognosis in hepatocellular carcinoma based on a unique immune response signature of the liver microenvironment. Cancer Cell 2006;10:99-111.
37. Seike M, Yanaihara N, Bowman ED, Zanetti KA, Budhu A, Kumamoto K, et al. Use of a cytokine gene expression signature in lung adenocarcinoma and the surrounding tissue as a prognostic classifier. J Natl Cancer Inst 2007 15;99:1257-1269.

Human Cancer Biology

Clinical Cancer Research

Integrative Array-Based Approach Identifies MZB1 as a Frequently Methylated Putative Tumor Suppressor in Hepatocellular Carcinoma

Satoshi Matsumura[1,5], Issei Imoto[1,7], Ken-ichi Kozaki[1], Takeshi Matsui[2], Tomoki Muramatsu[1,3], Mayuko Furuta[1,3], Shinji Tanaka[5], Michiie Sakamoto[6], Shigeki Arii[5], and Johji Inazawa[1,3,4]

Abstract

Purpose: The aim of this study was the identification of novel tumor suppressor genes (TSG) silenced by DNA hypermethylation in hepatocellular carcinoma (HCC).

Experimental Design: We conducted integrative array-based approach for genome-wide screening of methylation targets using a methylated DNA immunoprecipitation-CpG island microarray and expression array in three universal hepatoma cell lines and normal liver tissue. Through detailed expression and functional analyses using hepatoma cell lines and primary HCC samples, we isolated novel TSGs for HCC.

Results: A total of 642 genes were identified as methylated in three hepatoma cell lines but unmethylated in normal liver tissue, whereas 204 genes on autosomes were identified as genes unexpressed but restored after treatment with 5-aza-2′-deoxycytidine in these cell lines and expressed in normal tissue. Through the integration of results of the two-array analyses and further validation analyses of expression and methylation status in 17 cell lines and 30 primary tumors of hepatoma, we identified *MZB1, marginal zone B and B1 cell-specific protein*, encoding an endoplasmic reticulum protein, as a putative TSG frequently methylated within its CpG island in hepatoma. Among 162 patients with primary HCC, silencing of MZB1 protein was significantly and independently associated with a worse outcome. Restoration of MZB1 expression in hepatoma cells reduced cell proliferation *in vitro* and *in vivo* through G_1-arrest.

Conclusions: These results suggest that methylation-mediated silencing of MZB1 expression leads to loss of its tumor-suppressive activity, which may be a factor in the hepatocarcinogenesis, and is a useful prognosticator in HCC. *Clin Cancer Res; 18(13); 3541–51. ©2012 AACR.*

Introduction

Hepatocellular carcinoma (HCC), one of the most common malignancies worldwide, is associated with hepatitis virus infections, dietary aflatoxin, chronic alcohol/tobacco consumption, and cirrhosis. Genomic alterations, such as the gain or loss of chromosomal regions and specific gene mutations, have been frequently noted in hepatocarcinogenesis (1). Furthermore, epigenetic abnormalities, such as DNA methylation and chromosome remodeling, may also promote tumorigenesis (2, 3). DNA hypermethylation of promoter CpG islands leads to the inactivation of tumor suppressor genes (TSG) and critical cancer-related genes in human cancers including HCC (4, 5). DNA methylation changes have been reported to be specific to the cancerous tissue making it possible to distinguish HCC and surrounding nontumorous tissues (6). Indeed, abnormal DNA methylation of several TSGs, such as *RASSF1A*, *CDKN2A*, *CRABP1*, *GSTP1*, *CHRNA3*, *DOK1*, *SFRP1*, *GAAD45a*, and *CDKN2B*, is reported to be associated with HCC, and hypermethylation of specific genes, such as *CHFR* and *SYK* is detected in advanced stages of HCC (6). However, the number of reported methylation-target genes is far fewer for HCC than for colon cancer or gastric cancer (7). Therefore, further identification of remaining targets for methylation may clarify the specific molecular events involved in HCC progression, enabling the prevention, diagnosis, and treatment of HCC to be approached as potential clinical applications of DNA methylation signature at a molecular level.

To discover novel methylation-target sequences with high specificity and sensitivity in a genome-wide manner, large-scale screening methods, which have the potential to

Authors' Affiliations: [1]Department of Molecular Cytogenetics, [2]Medical Top Track Program, Medical Research Institute and School of Biomedical Science, [3]Global Center of Excellence Program for International Research Center for Molecular Science in Tooth and Bone Diseases, [4]Department of Genome Medicine, Hard Tissue Genome Research Center, and [5]Department of Hepato-Biliary-Pancreatic Surgery, Graduate School of Medicine, Tokyo Medical and Dental University; [6]Department of Pathology, School of Medicine, Keio University, Tokyo; and [7]Department of Human Genetics, Institute of Health Biosciences, The University of Tokushima Graduate School, Kuramoto-cho, Tokushima, Japan

Note: Supplementary data for this article are available at Clinical Cancer Research Online (http://clincancerres.aacrjournals.org/).

Corresponding Author: Johji Inazawa, Department of Molecular Cytogenetics, Medical Research Institute, Tokyo Medical and Dental University, 1-5-45 Yushima, Bunkyo-ku, Tokyo 113-8510, Japan. Phone: 81-3-5803-5820; Fax: 81-3-5803-0244; E-mail: johinaz.cgen@mri.tmd.ac.jp

doi: 10.1158/1078-0432.CCR-11-1007

Translational Relevance

Although hepatocellular carcinoma (HCC) is one of the most common malignancies worldwide, the molecular mechanisms underlying hepatocarcinogenesis remain unclear. Epigenetic abnormalities, such as DNA methylation, may promote tumorigenesis as well as genomic alterations in hepatocarcinogenesis. To discover novel methylation-target sequences with high specificity and sensitivity in a genome-wide manner, we conducted expression array analyses as well as methylated-DNA immunoprecipitation in combination with an oligonucleotide array, which allows for rapid and efficient genome-wide assessment of DNA methylation, resulting in the identification of *marginal zone B and B1 cell-specific protein (MZB1)* as a tumor suppressor gene silenced by DNA hypermethylation in hepatoma. Among 162 patients with primary HCC, silencing of MZB1 protein was significantly and independently associated with a worse outcome. Moreover, restoration of MZB1 expression in hepatoma cells reduced cell proliferation *in vitro* and *in vivo* through G_1 arrest. Our findings provide a novel insight into the prevention, diagnosis, and treatment of HCC.

find novel methylation targets in a whole range of cancers, have been developed. A combination of 3 types of pretreatments, such as enzyme digestion, affinity enrichment, or sodium bisulfite, was followed by different analytical steps, such as gel-, array-, or next-generation sequencing-based analysis (8). Among them, methylated-DNA immunoprecipitation (MeDIP; ref. 9) in combination with an oligonucleotide array or next-generation sequencing allows for rapid and efficient genome-wide assessment of DNA methylation, although these methodologies generally result in a list of several hundred candidate genes. Although an analysis of possible promoters or dense CpG islands is used to narrow down the number of candidate genes, the list is still too long. Pharmacologic unmasking expression microarray approaches are also used widely to identify methylation targets (10), although they are also prone to give false-positive genes that are indirect methylation targets themselves and not considered to be a reliable gauge of DNA methylation at a given locus.

To identify genes that are downregulated because of DNA hypermethylation and to concentrate those genes most frequently involved in HCC, we applied the following integrative array-based approach to 3 hepatoma cell lines: (i) MeDIP in combination with CpG island-array (MeDIP-chip) analysis to identify genes methylated in a cancer-specific manner, (ii) expression microarray analysis to identify genes downregulated in a cancer-specific manner and reactivated upon treatment with 5-aza-2′deoxycytidine (5-aza-dCyd), and (iii) a combination of data from both approaches. Through further examination of a subset of obtained candidates, we identified marginal zone B and B1 cell-specific protein (MZB1), also known as proapoptotic caspase adaptor protein (PACAP), pERp1, or MGC29506 (11), whose inactivation is related with a worse prognosis in primary tumors as a possible TSG for HCC.

Materials and Methods

Cell lines and primary tumor samples

A total of 17 hepatoma cell lines including 15 HCC lines (cHc4, Hep3B, Hep-Kano, Hep-TABATA, HLE, HLF, huH-1, HuH-7, JHH-1, JHH-4, JHH-5, JHH-7, Li-7, PLC/PRF/5, and SK-HEP-1) and 2 hepatoblastoma lines (HepG2 and HUH-6) were used (12). All 162 primary HCC samples were obtained during surgery from patients with HCCs treated at Tokyo Medical and Dental University (Tokyo, Japan) between 2000 and 2005. Relevant clinical and survival data were available for all patients (Table 1). The median follow-up period for the surviving patients was 19 months (ranging from 1 to 103 months). Samples from 17 of these patients with HCC were immediately frozen in liquid nitrogen and stored at −80°C until required for DNA and RNA analyses. Normal liver tissues were obtained from surgical samples in 2 patients (cases C20 and C40) with colon cancer metastasis. Written consent was obtained after approval by the local ethics committee.

MeDIP-chip analysis

The DNA methylation profiles were analyzed by MeDIP using anti-5-methylcytidine antibody (Eurogentec) followed by the Human 244K CpG island microarray (Agilent), which contains 237,220 probes, covering 27,800 CpG islands (97.5% of UCSC annotated CpG islands), according to the manufacturer's instructions. Image analysis with data extraction was done using Feature Extraction Software, version 9.0 (Agilent Technologies). The analytic procedure used for the results of the MeDIP-chip assay was described in the Supplementary Experimental Procedure.[1]

Gene expression array

Gene expression was profiled using a 4 × 44K Human Whole Genome Ver. 2.0 gene expression array (Agilent Technologies) according to the manufacturer's instructions. Total RNAs extracted from hepatoma cell lines and from these cells treated with 10 μmol/L 5-aza-dCyd for 5 days were used for conventional and pharmacologic unmasking analyses, respectively. Two normal livers (C20 and C40) were used as controls. All samples were analyzed twice. Image analysis with data extraction and the data analysis were conducted using Feature Extraction Software, version 9.0 and GeneSpring GX10 software (Agilent Technologies), respectively.[1]

Real-time reverse transcription PCR

To analyze the restored expression of genes, the cell lines were cultured with 1 to 10 μmol/L 5-aza-dCyd for 5 days. Levels of mRNA expression were measured with ABI PRISM

[1]The entire microarray data set is available at http://www.ncbi.nlm.nih.gov/geo/info/linking.html under the data series accession no. GSE35313.

Table 1. Association between clinicopathologic characteristics and MZB1 expression

		MZB1 immunoreactivity		
	n	Negative (%)	Positive (%)	*P* [a]
Total	162	84 (51.9)	78 (48.1)	
Gender				
Male	122	66 (54.1)	56 (45.9)	0.4139
Female	40	18 (45.0)	22 (55.0)	
Age, y				
Mean		65.7	65.7	
>65	98	49 (50.0)	49 (50.0)	0.5594
<65	64	35 (54.7)	29 (45.3)	
Virus				
HCV(+)	79	39 (49.4)	40 (50.6)	0.2742
HBV(+)	38	25 (65.8)	13 (34.2)	
HCV(−), HBV(−)	45	20 (44.4)	25 (55.6)	
AFP, ng/mL[b]		5,390 ± 22,968	2,819 ± 13,373	0.3982
PIVKA-II, mAU/mL[b]		7,252 ± 43,097	6,767 ± 25,669	0.9325
Aspartate aminotransferase, IU/L[b]		48.6 ± 25.3	54.7 ± 34.2	0.1982
Alanine aminotransferase, IU/L[b]		42.8 ± 32.6	53.7 ± 34.8	**0.0418**
Platelet (%)[b]		84.1 ± 13.1	85.9 ± 13.6	0.3862
Total bilirubin, mg/dL[b]		0.86 ± 0.44	0.86 ± 0.40	0.9795
Albumin, g/dL[b]		3.9 ± 0.5	3.9 ± 0.4	0.6972
Child–Pugh score[b]		5.4 ± 0.6	5.3 ± 0.7	0.8199
Tumor size, cm[b]		4.6 ± 2.8	4.5 ± 3.1	0.8411
Tumor number				
Single	105	50 (47.6)	55 (52.4)	0.1940
Multiple	57	34 (59.6)	23 (40.4)	
Histopathologic grading				
Well-differentiated	43	24 (55.8)	19 (44.2)	0.4560
Moderately differentiated	90	43 (47.8)	47 (52.2)	
Poorly differentiated	29	17 (58.6)	12 (41.4)	
Portal vein invasion				
Absent	92	40 (43.5)	52 (56.5)	**0.0222**
Present	70	44 (62.9)	26 (37.1)	
Surgical margin				
Absent	139	73 (52.5)	66 (47.5)	0.8478
Present	23	11 (47.8)	12 (52.2)	
Background liver parenchyma				
Normal liver	10	2 (20.0)	8 (80.0)	0.0696
Chronic hepatitis	78	39 (50.0)	39 (50.0)	
Liver cirrhosis	74	43 (58.1)	31 (41.9)	
Tumor stage				
I	13	3 (23.1)	10 (76.9)	**0.0207**
II	57	25 (43.9)	32 (56.1)	
III	58	33 (56.9)	25 (43.1)	
IVA	34	23 (67.6)	11 (32.4)	

NOTE: Statistically significant values are in boldface type.
Abbreviations: HBV, hepatitis B virus; HCV, hepatitis C virus.
[a]*P* values are from χ^2, Fisher exact, or Student *t* test and were statistically significant at <0.05.
[b]Mean ± SD.

7500 sequence detection System (Applied Biosystems) using TaqMan Gene Expression Assays (Hs01048042_m1 for *ANGPT2*, Hs00174937_m1 for *CCK*, Hs00405322_m1 for *DERL3*, Hs00417143_m1 for *RADIL*, Hs00191390_m1 for *KCNK6*, Hs00219458_m1 for *L1TD1*, Hs00414907_m1 for *MZB1*, Hs00386153_m1 for *FAR1*, Hs00382235_m1 for *OCIAD2*, Hs00257935_m1 for *PBX4*, and Hs00610060_m1 for *SFRP1*; Applied Biosystems)

according to the manufacturer's instructions. Gene expression values are given as ratios between the genes of interest and an internal reference gene (Hs99999903_m1 for *ACTB*; Applied Biosystems) that provides an internal normalization factor, and subsequently normalized with the value in the controls (relative expression level). The assay was conducted twice for each sample.

Methylation analysis

Sodium bisulfite-treated genomic DNA was subjected to PCR using primer sets to amplify regions of interest (Supplementary Table S1). For the combined bisulfite restriction analysis (COBRA), PCR products were digested with *Bst*U1, *Taq*1, or *Hha*1 and electrophoresed (13). The intensity of methylated alleles as a percentage on the ethidium bromide-stained gels was calculated, and a methylation density cutoff point of 20% was considered significant as described elsewhere (14). For bisulfite genomic sequencing (BGS), PCR products were subcloned and sequenced.

Immunohistochemistry

Indirect immunohistochemistry was conducted with formalin-fixed, paraffin-embedded tissue sections using an automated immunostainer (Benchmark XT; Ventana Medical Systems) with heat-induced epitope retrieval, anti-MZB1 (1:50; 11454-1-AP; Protein Tech), anti-PCNA (1:1,000; #2586; Cell Signaling Technology), or anti-Ki-67 antibodies (1:100; M7240; Dako). The slides were counterstained with Mayer's hematoxylin, and analyzed under a light microscope by 2 pathologists blinded to clinical characteristics and outcomes. Twenty representative fields per slide were examined, and the percentage of the total cell population that expressed MZB1 was evaluated for each case at ×200 magnification. Expression of MZB1 protein was graded as either positive (≥10% of tumor cells showing immunopositivity) or negative (±10% of tumor cells showing immunopositivity or no staining). Plasma cells and bile duct epithelial cells were used as positive and negative controls, respectively.

Western blotting

Western blotting was conducted as described elsewhere (12). Anti-FLAG-tag and anti-β-actin antibodies were purchased from Sigma-Aldrich, and the anti-cleaved caspase-3 antibody (#9661) was purchased from Cell Signaling Technology.

Fluorescent immunocytochemistry

The plasmid expressing C-terminally FLAG-tagged MZB1 (pCMV-3Tag3A-MZB1) was obtained by cloning the full coding sequence of MZB1 in-frame along with the 3xFLAG-epitope into the pCMV-3Tag3A vector (Stratagene). Cells were fixed in 10% trichloroacetic acid, permeabilized with 0.2% Triton X-100, and treated with blocking solution (1% bovine serum albumin in PBS). After incubation with the primary antibodies (anti-MZB1, 1:100 and/or anti-Calnexin, 1:100) for 1 hour, the bound antibody was visualized using a Cy3-conjugated or fluorescein isothiocyanate (FITC)-conjugated secondary antibody (1:1,000). After being mounted with DAPI (4′,6′-diamidino-2-phenylindole) to stain nuclei, the cells were observed under a fluorescence microscope (BZ-8100; Keyence).

In vitro and *in vivo* growth assay

Colony formation assays using cells transiently introduced with pCMV-3Tag3A-MZB1 or the empty vector (pCMV-3Tag3A-mock) was conducted as described elsewhere (15). The expression of MZB1 protein was confirmed 48 hours after transfection by Western blotting and fluorescent immunocytochemistry.

Stable MZB1 transfectants and control counterparts were obtained by introducing pCMV-3Tag3A-MZB1 or pCMV-3Tag3A-mock into cells with G418 selection, and 2.5×10^4 cells were seeded in 24-well plates. The numbers of viable cells were assessed 24 to 72 hours after seeding by the water-soluble tetrazolium salt assay. The cell cycle was evaluated 48 hours after seeding by a fluorescence-activated cell sorting (FACS) as described elsewhere (15).

The *in vivo* tumor-suppressive ability of MZB1 was investigated by conducting tumor xenograft experiments. Six-week-old female severe combined immunodeficient (SCID) mice were injected subcutaneously in the lower back with MZB1-expressing or control mock-transfected cells (4×10^7). All procedures involving animals were approved by and conformed to the guidelines of our Institutional Animal Care and Use Committee. Tumor formation in SCID mice was monitored daily and the recipient mice were sacrificed for tumor weight evaluation and protein expression analyses 5 weeks postinjection.

Statistical analysis

The χ^2 or Fisher's exact test was used to test for differences between groups. Kaplan–Meier method and log-rank test were used for the survival analyses. Univariate and multivariate survival analyses were conducted using the likelihood ratio test of the stratified Cox proportional-hazards model. Differences between subgroups were tested with the Student *t* test. For multiple group comparisons, ANOVA followed by Scheffé *post-hoc* test was used. Differences were assessed with a 2-sided test, and considered significant at the $P < 0.05$ level.

Results

Screening in the MeDIP-chip analysis

For the screening of aberrantly methylated genes by MeDIP-chip analysis, we used a CpG island microarray, in which 11,229 genes harbor CpG islands upstream or within, with the algorithm shown in the Supplementary Experimental Procedure and Supplementary Fig. S1. Among 11,229 genes, CpG islands of 2,476 genes were unmethylated in normal liver tissue (case C20) but methylated in at least 1 of 3 hepatoma cell lines (Hep3B,

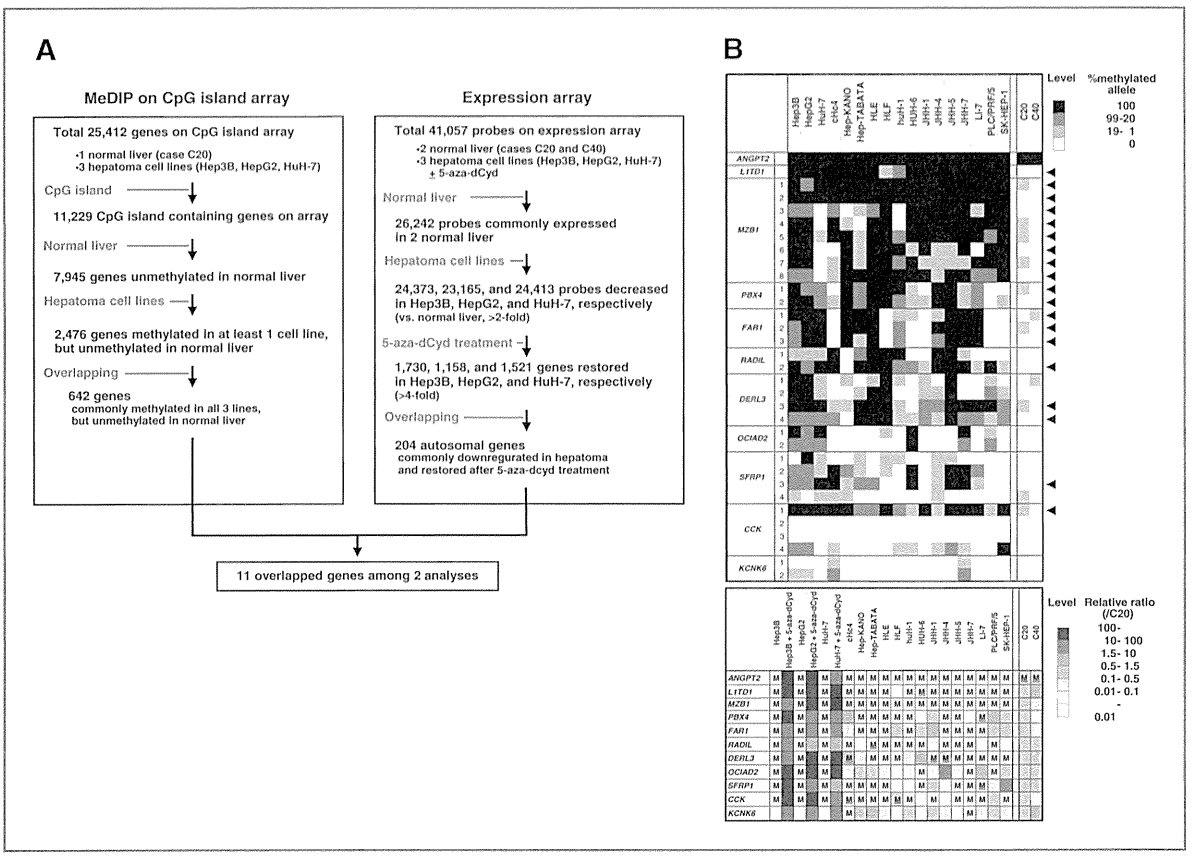

Figure 1. Identification of 11 genes as possible methylation targets. A, left top, overview of the screening approach using MeDIP-chip analyses in 3 hepatoma cell lines (Hep3B, HepG2, and HuH-7) and control normal liver tissue (case C20); right top, overview of the screening approach using duplicate expression array analyses in the same 3 hepatoma cell lines without and with 5-aza-dCyd treatment and 2 normal liver tissues (cases C20 and C40); bottom, by combining results obtained from 2 different genome-wide array-based screening methods, 11 genes overlapped between 2 approaches as possible genes, which are consistently silenced by tumor-specific CpG island methylation. B, top, summary of DNA methylation status of CpG islands around 11 selected candidates in 17 hepatoma cell lines and normal liver tissue determined by COBRA. Each box indicates restricted status by enzymes (% methylated allele). A methylation density cutoff point of 20% was considered significant (13). Arrowheads indicate regions in which more than 50% (>9 of 17) of cell lines showed tumor-specific hypermethylation compared with normal liver tissue; bottom, profiles of expression of 11 candidates determined by real-time RT-PCR in 17 hepatoma cell lines. Three (Hep3B, HepG2, and HuH-7) of 17 lines were treated with 5-aza-dCyd. Ratio relative to normal liver tissue (C20) is shown by a 7-gradient pattern. "M's" indicates that genes showed hypermethylation (see C, top) in each cell line: nonunderlined and underlined "M's" indicate silenced (<0.01 compared with C20) and retained gene expression, respectively.

HepG2, and HuH-7). Because CpG islands of 642 of those 2,476 genes were methylated in all 3 cell lines (Fig. 1A), we selected them as candidates consistently hypermethylated in hepatomas.

Screening in the expression array analysis

In expression array analysis done in a duplicate manner, we used only reproducible probes (the coefficient of variation, CV <50%) in each set of experiments to evaluate obtained values. We focused on genes satisfying 2 criteria: (a) genes whose expression was observed in normal liver tissue but repressed in hepatoma cells, and (b) genes whose expression was restored after treatment with 5-aza-dCyd in hepatoma cells. Among genes expressed in normal liver tissue (C20 and C40), the expression of 1,730, 1,158, and 1,521 genes was silenced but restored by 5-aza-dCyd in Hep3B, HepG2, and HuH-7 cells, respectively. Among them, 204 genes on autosomes commonly satisfied criteria in all 3 lines (Fig. 1A), indicating 204 genes to be candidates consistently silenced through methylation in hepatocarcinogenesis.

Integration and validation of results in two microarray-based analyses

On the basis of the MeDIP-chip and expression array analyses, 11 genes were selected as overlapping genes in 2 different genome-wide array-based screening methods, suggesting them to be pharmacologically unmasked, tumor-specific methylation targets in all 3 hepatoma cell lines (Fig. 1A and Supplementary Table S2). Because these genes seem to be silenced in a tumor-specific manner, they are also candidates for TSG in hepatocarcinogenesis.

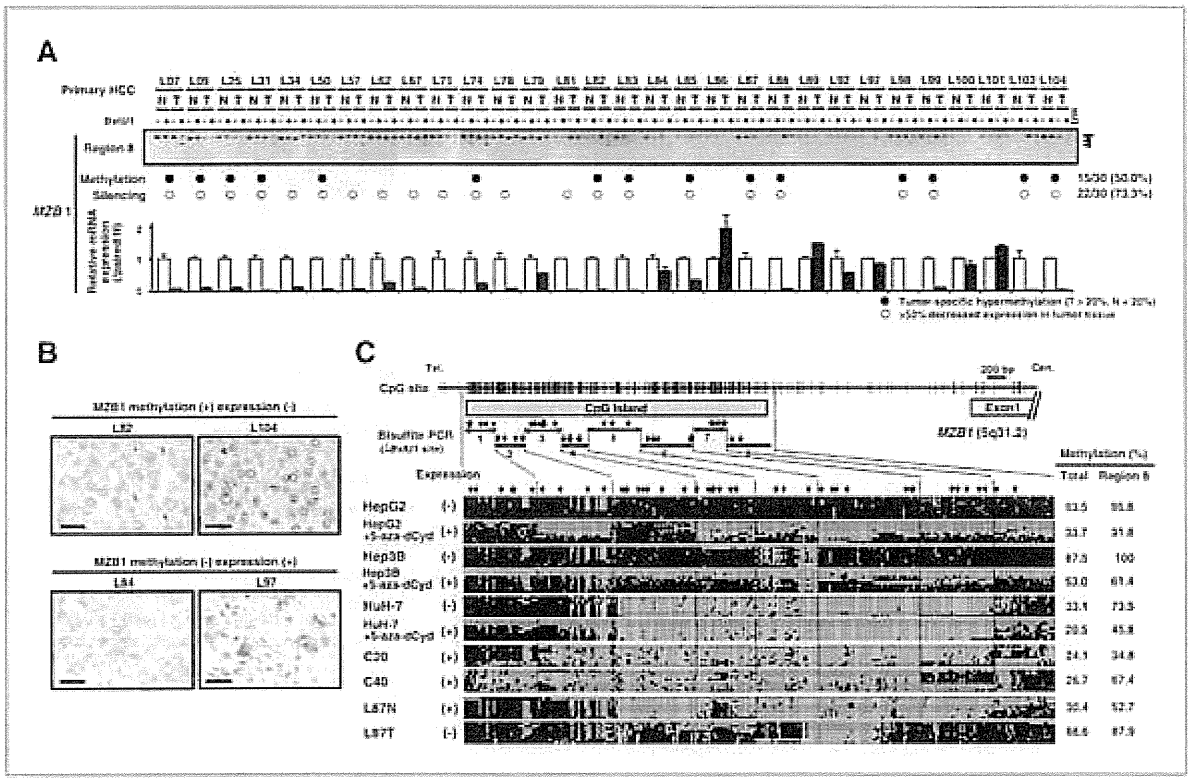

Figure 2. Correlation of methylation and expression status of MZB1 in primary HCCs. A, representative results of the methylation status of region 8 within the *MZB1* CpG island determined by COBRA (top) and the relative level of *MZB1* mRNA expression determined by real-time RT-PCR (bottom) in primary HCC tumors (T) and corresponding noncancerous liver tissues (N). Arrowheads, fragments specifically restricted at sites recognized as methylated CpGs; arrow, undigested fragments indicating unmethylated CpGs. A methylation density of cutoff point of 20% was considered significant (14). Closed and open circles indicate samples with tumor-specific methylation (positive in tumor but negative in corresponding nontumorous tissue) and those with the reduced mRNA expression (>50% decreased expression) in tumor tissue compared with paired nontumorous tissue, respectively. B, representative results of immunohistochemical analysis of MZB1 protein expression in primary HCCs indicate that methylation status of *MZB1* is inversely correlated with its mRNA and protein expression. Bars, 20 μm. Magnifications are ×200. C, top, a schematic map of the CpG-rich region around the CpG island and exon 1 of *MZB1*. Vertical ticks, CpG sites on the expanded axis. Gray box, CpG island. Horizontal closed arrows, the regions examined in the COBRA and BGS. Downward arrows, restriction sites (BstU1) for the COBRA. Bottom, representative results of BGS of the *MZB1* CpG island in 3 hepatoma cell lines without and with 5-aza-dCyd, 2 normal livers (C20 and C40), and a paired representative case (cases L87) examined in the COBRA. Open and filled squares represent unmethylated and methylated CpG sites, respectively, and each row represents a single clone. Restriction sites are indicated by downward arrows.

We then determined the status of methylation and expression for all 11 candidates through COBRA and real-time reverse transcription PCR (RT-PCR), respectively, in a panel of 17 hepatoma cell lines and 2 normal liver tissues (Fig. 1B). Among them, *ANGPT2* was highly methylated in both the hepatoma cells and normal liver tissue. Among the other 10 genes, 8 genes (*LITD1*, *MZB1*, *PBX4*, *FAR1*, *RADIL*, *DERL3*, *SFRP1*, and *CCK*) harbored at least 1 hypermethylated region in >50% of hepatoma cell lines compared with normal liver tissue, whereas *OCIAD2* and *KCNK6* were infrequently methylated in the hepatoma lines. Among those 8 genes, only *MZB1* and *FAR1* were downregulated (<0.1 relative to normal liver) in all cell lines with their hypermethylation, whereas the other 6 genes were expressed even in cell lines with their hypermethylation, suggesting *MZB1* and *FAR1* to be possible methylation targets for gene silencing in hepatoma cells, although the expression of all 11 genes was more or less restored by 1 to 10 μmol/L of 5-aza-dCyd treatment in each of the 3 cell lines (Supplementary Fig. S2).

MZB1 is frequently silenced through CpG island methylation in primary tumors

We next determined the methylation and expression status of *MZB1* and *FAR1* in 17 paired tumorous and nontumorous tissues from primary HCCs (cases L81-L104; Fig. 2A and Supplementary Fig. S3). Tumor-specific *MZB1* (region 8) and *FAR1* (region 3) hypermethylation was observed in 9 (52.9%) and 8 (47.1%) cases, respectively. In those cases with hypermethylation, tumor-specific downregulation of *MZB1* and *FAR1* expression was observed in 9/9 (100%) and 5/8 (62.5%) cases, respectively, suggesting *MZB1* to be the most probable candidate for a gene silenced through tumor-specific methylation. In additional 13 cases (Fig. 2A, cases L07-L79), tumor-specific *MZB1* hypermethylation was observed in 6 (46.2%) cases

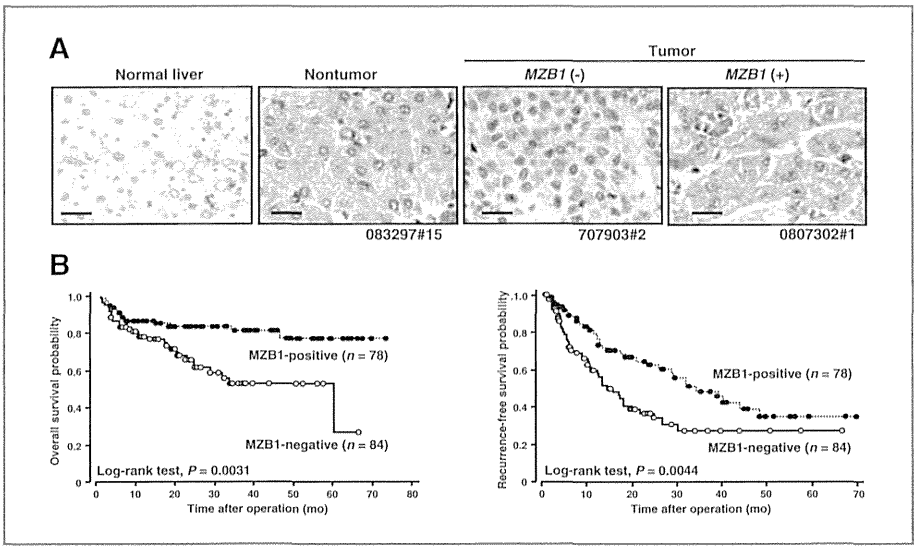

Figure 3. A, representative results of immunohistochemical staining of MZB1 protein in normal liver tissue, nontumorous liver tissue, and tumorous tissues in HCCs. Both normal and nontumorous hepatocytes showed MZB1 immunopositivity, whereas tumor cells showed either negative or positive immunoreactivity. Bars, 25 μm. Magnifications are ×200. B, Kaplan–Meier curves for overall survival (left) and recurrence-free survival (right) rates of 162 patients with primary HCCs. Negative MZB1 immunoreactivity of tumor cells was significantly associated with worse overall and recurrence-free survivals ($P = 0.0031$ and 0.0044, respectively; log-rank test).

and all of those cases also showed tumor-specific downregulation of this gene. Among 12 cases available for immunohistochemical staining of MZB1 protein, MZB1 was expressed in nontumorous tissues and the methylation status and protein expression status of MZB1 matched in 8 tumorous tissues (Fig. 2B).

To clarify the methylation status of the CpG island of *MZB1*, we conducted BGS in cell lines and tumorous and nontumorous tissues of HCC as well as normal liver tissue. CpG sites within the CpG island tended to be differentially methylated among the cell lines and primary samples: MZB1-nonexpressing cell lines except HuH-7 and primary tumors showed a highly methylated pattern within the CpG island, whereas MZB1-expressing normal liver tissue and nontumorous tissue of HCC case showed partially methylated (Fig. 2C). Although total %methylation of CpG sites within the CpG island of HuH-7 cells is higher than but close to those in MZB1-expressiong samples, dense methylation without unmethylated allele was observed in specific regions within CpG island in HuH-7 cells. In addition, we confirmed that treatment with 5-aza-dCyd partially restored methylation within the CpG island of *MZB1* in HepG2, Hep3B, and HuH-7 cells, whose expression of MZB1 was restored after the same treatment (Fig. 1B), suggesting that methylation within the CpG island upstream to *MZB1* occurs in cell lines and primary tumors of hepatoma and at least partly contributes to the silencing of its expression of the mRNA and protein level. Notably, 5-aza-dCyd-treated hepatoma cells and C20 showed similar methylation level of the *MZB1* CpG island (Fig. 2C), whereas 5-aza-dCyd-treated hepatoma cells showed much higher MZB1 expression level compared with C20 (Fig. 1B), suggesting that 5-aza-dCyd treatment indirectly activates transcription of MZB1 through demethylation of transcription factors/cofactors for MZB1, which might downregulated in normal hepatocytes or other mechanisms.

Immunohistochemical staining of MZB1 in primary HCCs

To determine clinicopathologic significance of the MZB1downregulation in primary HCCs, we conducted an immunohistochemical analysis of the MZB1 in 162 primary cases (Fig. 3 and Table 1). In the tumorous regions, 78 (48.1%) showed immunoreactivity to MZB1 (positive in Table 1), whereas 84 (51.9%) did not (negative in Table 1). In the nontumorous regions, on the other hand, 135 (83.3%) showed immunoreactivity to MZB1, whereas 27 (16.7%) did not. Negative MZB1 immunoreactivity was more frequent in cases with portal invasion ($P = 0.0222$) and in higher tumor stages ($P = 0.0207$). However, the MZB1 protein expression in each tumor was not associated with other characteristics.

In Kaplan–Meier survival curves, univariate analyses of overall and nonrecurrent survival with log-rank tests showed a significant association between negative MZB1 immunoreactivity and a poor survival rate of patients ($P = 0.0031$ and 0.0044, respectively; Fig. 3B). In the Cox proportional hazard regression model (Table 2), univariate analyses showed that negative MZB1 immunoreactivity, α-fetoprotein (AFP), tumor size, tumor number, portal vein invasion, background liver parenchyma, and tumor stage were significantly associated with overall survival. Multivariate analysis using a stepwise

Table 2. Cox proportional hazard regression analysis for overall survival

	Univariate		Multivariate[a]
Factor	**HR (95% CI)**	***P*[a]**	***P*[b]**
Gender			
Male vs. female	0.990 (0.509–1.925)	0.9764	X
Age, y			
>65 vs. <65	0.957 (0.527–1.738)	0.8859	X
AFP			
>200 vs. <200 ng/mL	2.202 (1.214–3.995)	**0.0094**	X
Tumor size			
>3 vs. <3 cm	3.548 (1.498–8.401)	**0.0040**	**0.0319**
Tumor number			
Multiple vs. single	2.531 (1.406–4.554)	**0.0019**	X
Histopathologic grading			
Poor-moderate vs. well	2.312 (1.074–4.975)	0.0321	X
Portal vein invasion			
Present vs. absent	2.309 (1.136–3.716)	**0.0173**	X
Surgical margin			
Present vs. absent	1.948 (0.963–3.940)	0.0637	X
Background liver parenchyma			
LC vs. CH + NL	1.825 (1.009–3.300)	**0.0468**	X
Stage			
III + IVA vs. I + II	3.466 (1.710–7.024)	**0.0006**	**0.0301**
MZB1 expression[c]			
Negative vs. positive	2.532 (1.338–4.791)	**0.0043**	**0.0234**

NOTE: Statistically significant values are in boldface type.

Abbreviations: CH, chronic hepatitis; LC, liver cirrhosis; NL, normal liver.

[a]Forward and backward stepwise analyses were used for multivariate analysis.

[b]*P* values are from 2-sided tests and were statistically significant at <0.05.

[c]MZB1 expression was evaluated by immunohistochemical analysis as described in Materials and Methods.

Cox regression procedure revealed that MZB1 immunoreactivity, tumor size, and tumor stage were independently selected as predictive factors for overall survival in both forward and backward procedures ($P = 0.0234$, 0.0319, and 0.0301, respectively).

MZB1 reexpression suppresses proliferation and tumor formation of cancer cells *in vitro* and *in vivo*

To investigate the biologic significance of MZB1 in hepatocarcinogenesis, MZB1 expression was transiently or stably restored in hepatoma cells lacking MZB1 expression. We then measured the proliferation and tumor formation of those cells in comparison with the control counterparts transduced with an empty vector *in vitro* and *in vivo*.

In colony-formation assays using transiently transfected cells, the occupancy of the stained area of colonies produced by MZB1-transfected HLE cells (Fig. 4A), which show *MZB1* hypermethylation pattern (Supplementary Fig. S4), and other hepatoma cells (data not shown) decreased compared with those of control counterparts. In an *in vitro* proliferation assay using stably transfected cells, cells expressing MZB1 protein, which was predominantly colocalized with an endoplasmic reticulum (ER) marker in the cytoplasm, grew slightly but significantly slower than the control cells (Fig. 4B). In a FACS analysis to examine the mode of action of MZB1 in the cell cycle, an accumulation of cells in G_0–G_1 phase and a decrease in S and G_2–M phase cells but no increase in sub-G_1 phase cells was observed among MZB1-transfected cells compared with mock-transfected counterparts (Fig. 4C), suggesting that MZB1 contributes to the arrest of hepatoma cells at the G_1-S checkpoint without inducing apoptosis. Indeed, a similar expression pattern of cleaved caspase 3, one of markers of apoptosis, was observed between stable MZB1 transfectants and control counterparts even after treatment with CDDP for induction of apoptosis (Fig. 4C). Subcutaneous tumor growth experiments using stable transfectants showed that restored expression of MZB1 in hepatoma cells correlated with reduced tumor volume and weight *in vivo* probably because of a decrease in cell proliferation shown by lower PCNA and Ki-67 positivities in MZB1-transfected cells (Fig. 4D). In resected tumors, no induction of apoptosis detected by

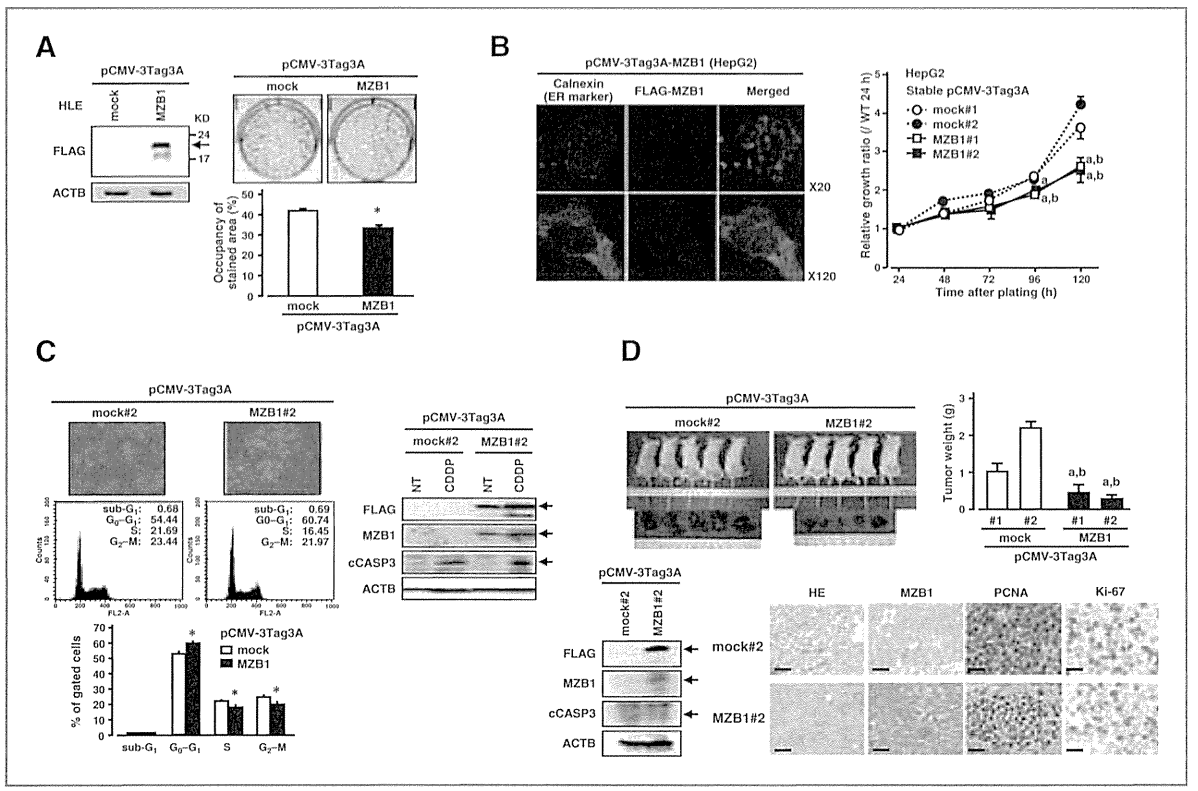

Figure 4. Tumor-suppressive effects of restoration of MZB1 expression in hepatoma cells *in vitro* and *in vivo*. A, HLE cells lacking MZB1 expression were transiently transfected with pCMV-3Tag3A-MZB1 or pCMV-3Tag3A-mock and selected with G418 for 2 weeks. MZB1 expression was confirmed by immunoblotting using 10 μg of protein extract and anti-MZB1 antibody (left). The drug-resistant colonies formed by the MZB1-transfected cells were more numerous than those formed by control counterparts (top right). Occupancy of the stained colony area was calculated (bottom right). Columns, means of 3 separate experiments, each conducted in triplicate; bars, SD (histogram). *, $P < 0.05$ versus mock control (Student *t* test). Similar results were obtained in the Hep3B and SK-HEP-1 cell lines (data not shown). B, stable HepG2 transfectants were established by transfection of pCMV-3Tag3A-MZB1 or pCMV-3Tag3A-mock with G418 selection. Immunofluorescence cytochemistry showed almost all pCMV-3Tag3A-MZB1–transfected cells to express FLAG-tagged MZB1 predominantly with an endoplasmic reticulum (ER) marker (calnexin, left). After plating into 24-well plates (2.5×10^4 cells per well), the proliferative activity of stably MZB1-transfected cells was found to be less than that of the control counterparts. Results of relative growth ratio are shown with the mean ± SD for 3 separate experiments, each done in triplicate (right). Differences were analyzed by 1-way ANOVA with subsequent Scheffé tests: a and b, $P < 0.05$ versus mock #1 and #2, respectively. C, top left, representative results of the population in each phase of the cell cycle in stable transfectants described in (B) assessed by FACS. Bottom left, columns, means of 3 separate clones, each conducted in triplicate; bars, SD (histogram). *, $P < 0.05$ versus mock control (Student *t* test). Right, representative results of immunoblotting of MZB1 protein and cleaved caspase-3 (cCASP3), one of apoptotic markers, without (no treatment, NT) or with cisplatinum (CDDP, 20 μmol/L) treatment for 48 hours. D, representative results of tumors formed in SCID mice following injection of stably MZB1-transfected cells. MZB1-transfected HepG2 cells or mock-transfected cells (4×10^7) were injected into the right and left dorsal flanks. SCID mice were sacrificed for tumor weight evaluation 5 weeks postinjection (top left). Results of tumor weight are shown with the mean ± SD for 3 separate experiments, each done in triplicate (top right). Differences were analyzed as described in (B). Bottom left, representative results of immunohistochemical analysis of MZB1 as well as PCNA and Ki-67, markers for cell proliferation, in resected tumors. A positive MZB1 immunoreactivity was detected in MZB1-transfetced cells but not in mock-transfected counterparts, and both PCNA and Ki-67 immunoreactivities were less frequently observed in MZB1-transfetced cells compared with mock-transfected counterparts. Bars, 25 μm. Magnifications are ×200. Bottom right, representative results of immunoblotting of MZB1 protein and cCASP3 in resected tumors.

cleaved caspase 3 expression in MZB1-transfetced cells was observed compared with mock-transfected counterparts *in vivo* (Fig. 4D).

Discussion

Epigenetic silencing of TSGs plays an important role in the carcinogenesis (16), including hepatomagenesis (5–7). Although many studies have reported aberrant hypermethylation of genes in HCC, e.g. *CDH1*, *RASSF1A*, *GSTP*, *SOCS1*, *SFRP1*, and *PTEN* identified as TSGs silenced by hypermethylation, most of these studies were limited to the analysis of a single or a few genes (5–7, 17). Because the number of methylation-target TSGs identified to date is far fewer for HCC than for other cancers possibly because of fewer attempts to conduct genome-wide analysis (18), there remain many genes hypermethylated in HCC. With advancements in microarray technology, the number of genes found to be hypermethylated in HCC in a cancer-specific manner is

expected to increase (8, 19). Although the functional consequence of promoter hypermethylation is transcriptional silencing of the associated gene, this assumption often goes untested, as few have concurrently investigated both methylation and expression (6, 7). On the basis of these hypotheses and background, we conducted genome-wide screening of methylation-target TSGs using a combination of 2 microarray-based approaches: MeDIP-chip analysis in hepatoma cell lines and expression array analysis for genes pharmacologically unmasked in the same lines. As a result of this approach, several genes were newly identified as candidate methylation targets, and among them MZB1 was showed to be the most possible TSG, which is silenced through methylation and contributes to the hepatocarcinogenesis.

Among 11 genes we identified through genome-global screening of methylation-mediated silenced genes in hepatoma cells, 10 were newly identified candidates and only SFRP1 was known as possible methylation-target TSG in HCC (20, 21). The remarkable reduction in the number of candidate genes and lack of various known HCC-related methylation targets within candidates may be because of a small number of commonly methylated and/or silenced genes among the 3 cell lines used in this study. Indeed, several frequently methylated genes, such as SLIT2, PTGS2 (COX2), and HHIP, for which methylation data are available in all 3 hepatoma cell lines, showed different methylation patterns among the cell lines (22–24). These variations may come from the different backgrounds of the 3 cell lines, such as hepatitis B virus infection in Hep3B and no hepatitis virus infection in the other 2 lines, because hypermethylated genes in HCC tumors are known to exhibit remarkably distinct patterns depending on associated risk factors (25, 26). Therefore, it is suggested that the candidate genes identified and validated in the present study may contribute to functional pathways shared among different subtypes of HCC regardless of associated risk factors, and this might be the reason why MZB1 protein expression status was not statistically associated with the status of hepatitis virus infection and background liver parenchyma in our analysis.

One of striking findings of our immunohistochemical analysis of MZB1 using a panel of primary tumor samples of HCC was that immunoreactivity to the MZB1 protein in each sample was significantly associated with a worse clinical outcome even after stratification with other clinicopathologic characteristics. This result indicates that MZB1 might be useful as an independent prognosticator in patients with HCC, although MZB1 immunoreactivity in each case was significantly associated with portal invasion and in tumor stages. Because MZB1 seems to be downregulated in a cancer-specific manner in HCC and its expression is observed in most normal human tissues (11), it will be interesting whether MZB1 works as a TSG in specific tissues including liver or in various tissues.

MZB1 was first identified as a caspase-2–binding molecule through a yeast 2-hybrid system using a human B lymphocyte cDNA library, which was conducted to determine the mechanism of activation of caspase-2 in apoptosis of B cells triggered by ligation of the antigen receptor (11). Although MZB1 was shown to bind caspase-2 and -9 *in vitro* and *in vivo* and be triggered upon the transient transfection of human kidney cells and Rat-1 fibroblasts and stable transfection of human B cell lines (11), the precise mechanisms by which it exerts proapoptotic activity remain unclear because of the absence of structural hallmarks besides a CXXC thioredoxin motif and no homology with other molecules in apoptotic pathways. Recently, it was shown that MZB1 occurs in the luminal ER and affects multiple cellular processes, such as (a) the oxidative folding and assembly and secretion of immunoglobulin in plasma cells (27, 28) and (b) the regulation of Ca^{2+} homeostasis and ER Ca^{2+} stores, integrin-mediated adhesion, and antibody secretion in marginal zone B cells of the spleen and innate-like B cells (B1 cells, ref. 29). Because those processes are associated with the functional differentiation of B cells, it is possible that the MZB1-induced assembly of several target proteins including integrin may contribute to the antiproliferative effect of MZB1 on hepatoma cells without induction of apoptosis observed in this study. The expression of this gene is observed not only in the B-cell lineage including plasma cells, marginal zone B cells, or B1 cells (27–29), but also in most normal human tissues except the placenta constitutively even in the absence of an apoptotic stimulus (11), suggesting MZB1 to affect various biologic processes in different tissues possibly through interaction with various proteins and/or the targeting of various molecules. Indeed, MZB1 protein was reported to be downregulated in intestinal-type gastric cancer, although the clinicopathologic and biologic significance was not analyzed (30), suggesting MZB1 to act as a TSG at least in some tissues including stomach and liver tissue. Further examination will be required to clarify the mechanisms of the antiproliferative effect of MZB1.

Disclosure of Potential Conflicts of Interest

No potential conflicts of interest were disclosed.

Authors' Contributions

Conception and design: S. Matsumura, I. Imoto, J. Inazawa
Development of methodology: S. Matsumura, I. Imoto, T. Matsui, J. Inazawa
Acquisition of data: S. Matsumura, M. Furuta, S. Tanaka
Analysis and interpretation of data: S. Matsumura, I. Imoto, K. Kozaki, J. Inazawa
Writing, review, and/or revision of the manuscript: S. Matsumura, I. Imoto, J. Inazawa
Administrative, technical, or material support: I. Imoto, T. Muramatsu, M. Sakamoto, J. Inazawa
Study supervision: I. Imoto, T. Matsui, S. Arii, J. Inazawa

Acknowledgments

The authors thank Ayako Takahashi, Rumi Mori, and Ayumi Shioya for technical assistance.

Grant Support

This study was supported in part by Grant-in-Aid for Scientific Research (A) and (C), and Scientific Research on Priority Areas and Innovative Areas,